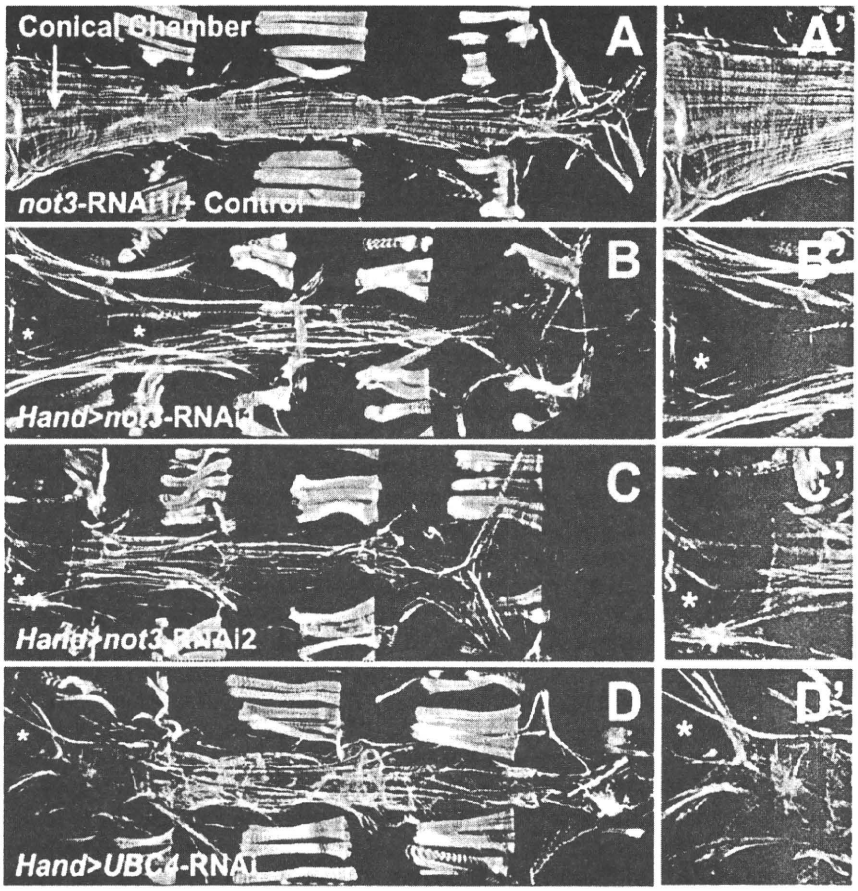

Figure 4. *not3* and *UBC4* Cardiac-Specific RNAi Knockdown Substantially Perturb Myofibrillar Organization and Content

(A) Alexa584-phalloidin staining of control *Drosophila* cardiac tubes reveals typical spiraling myofibrillar arrangements within the cardiomyocytes. The fibers, especially those in the conical chamber, located anteriorly, are densely packed with F-actin.

(B–D) Relative to control hearts, *not3* or *UBC4* RNAi knockdown severely disrupts myofibrillar organization and leads to an apparent loss of myofilaments as noted by large gaps in F-actin staining (*) as well as by a lack of myosin heavy chain transcripts (Figure S3F).

(A′–D′) Enlarged images of the conical chambers from (A)–(D), respectively, which illustrate the high degree of myofibrillar disarray and large gaps in F-actin staining within the cardiomyocytes of *not3* and *UBC4* RNAi knockdown hearts. Original images were taken at 10× magnification with a Zeiss Imager Z1 fluorescent microscope.

(*Serca2a*, *ATP2A2*), myosin heavy chain (*mhc*, *MYH7*), and the potassium channel *KCNQ* (*kcnq1*, *KCNQ1*) (Figure S3) involved in heart rhythm control. Cardiac-specific knockdown of *not3* increased the number of flies exhibiting contractile irregularities (Figures S3H and S3I), a finding similar to what is seen in response to cardiac-specific knockdown of the *KCNQ* K^+ channel (Figure S3I) and what has been reported for *KCNQ* mutant flies (Ocorr et al., 2007b). Of note, a *not3 P* element mutant was developmentally lethal, exhibiting a late stage defect in embryonic heart tube organization, which could be rescued by *P* element excision (Figure S3C).

The CCR4-Not complex component *UBC4* was also a major hit identified by our heart screen. Moreover, *UBC4* expression was reduced after *not3* knockdown (Figure S3B). *Hand-Gal4>UAS-UBC4*-RNAi flies also exhibited significantly longer heart periods and showed dramatically altered diastolic and systolic diameters and reduced fractional shortening relative to control hearts (Figures 3C–3G). Fluorescent imaging again revealed severe myofibrillar disarray (Figure 4D) that was strikingly similar to that observed in *not3* knockdown hearts. Further, we observed similar structural and functional phenotypes in *not1* cardiac-specific knockdown flies (A.C., G.N., J.P., and R.B., unpublished data). Thus, knockdown of different components of the CCR4-Not complex result in abnormal heart structure and severely impaired cardiac function indicative of dilated cardiomyopathy.

Functional Assessment of Additional *Drosophila* Heart Hits

To extend our confirmations beyond the CCR4-Not complex, we assayed heart function in adult flies with heart-specific knockdown of four additional candidates identified in our heart screen (Figure S3). One candidate heart gene tested was *CG1216* (*Mrityu*), which encodes a mesoderm-expressed BTB-POZ domain-containing protein (Rusconi and Challa, 2007). Cardiac knockdown of *CG1216* resulted in a significant increase in systolic diameter. Another candidate heart gene, *CG8933* (*extradenticle*), encodes a PBX-family transcription factor. Cardiac knockdown of *CG8933* resulted in increased systolic diameter and reduced fractional shortening. Cardiac knockdown of *CG33261* (*Trithorax-like*) resulted in significantly altered diastolic and systolic diameters as well as impaired fractional shortening. Finally, knockdown of *CG7371*, which encodes a Vps52 domain-containing protein predicted to participate in Golgi trafficking, resulted in a marked increase in heart period and affected the diastolic diameter. These data further demonstrate that our screen indeed has the capacity to identify novel factors involved in and required for normal adult heart function.

Generation of *not3* Knockout Mice

We next tested whether our data on *Drosophila* can be directly translated into a mammalian species. The mouse and human NOT3 proteins (official gene name *Cnot3*) share 60% identity with the *Drosophila not3* ortholog. Expression of human and mouse *not3* messenger RNA (mRNA) transcripts can be found in the majority of tissues analyzed. Although *not3* is evolutionarily conserved from yeast to mammals, essentially nothing is known about the in vivo role of mammalian *not3*. We therefore generated *not3* knockout mice.

We disrupted the *not3* gene in murine embryonic stem cells (ESCs) using a targeting vector in which nucleotides encompassing exons 2 through 9 are deleted (Figure 5A and Figure S4A). Both $not3^{+/-}$ male and $not3^{+/-}$ female mice are viable and exhibit normal fertility. We never obtained viable $not3^{-/-}$ newborn mice, indicating that loss of *not3* results in embryonic lethality. We staged embryonic development but failed to recover *not3* null embryos from placental implantations (Figures S4B and S4C). We therefore assayed early embryogenesis and observed that $not3^{-/-}$ blastocysts can develop. These mutant blastocysts have a normal appearance (Figure S4D), occur at Mendelian frequencies (Figures S4E and S4F), and express key markers of early embryonic differentiation at normal levels (Figure S4G). *not3* mRNA transcripts and NOT3 protein were undetectable in $not3^{-/-}$ blastocysts by RT-PCR and immunostaining (Figures S4F and S4G). In $not3^{+/+}$ and $not3^{-/-}$ epiblast cultures (Figure S4H), trophoblast cells started to spread and supported the outgrowths of the inner cell mass (ICM). While the ICM of $not3^{+/+}$ blastocysts continued to grow, $not3^{-/-}$ ICM cells exhibited a severe outgrowth defect. Thus, complete loss of mouse *not3* results in early embryonic death at the implantation stage.

not3 Haploinsufficiency Results in Impaired Heart Function

We speculated that similar to RNAi-mediated downregulation of *not3* in *Drosophila*, *not3* haploinsufficiency might also reveal a role in mammalian heart function. In *not3* heterozygote mice, *not3* expression is indeed downregulated in the heart (Figure 5B). We failed to observe overt structural changes in the hearts of $not3^{+/-}$ mice. However, both male and female *not3* haploinsufficient mice exhibited a reduction in cardiac contractility as determined by decreased left ventricle fractional shortening and increased left ventricular diameter in systole (Figures 5C and 5D).

To address whether the defects in cardiac function are intrinsic to the heart per se or whether the observed impairment of contractility was secondary because of haploinsufficiency of *not3* in other tissues, we subjected explanted hearts from wild-type and $not3^{+/-}$ littermate mice to Langendorff perfusion, assessing ex vivo heart function (Joza et al., 2005). When isoproterenol was used to activate β-adrenergic receptors, $not3^{+/-}$ hearts exhibited severe contractile abnormalities as defined by impaired generation of left ventricular pressure (LVP) (Figure 5E and Figure S5A). Hemodynamic measurements confirmed that all functional heart parameters such as dP/dT_{max} or dP/dT_{min}, indicative of generated contractile pressure, were markedly reduced in $not3^{+/-}$ hearts (data not shown). Moreover, when explanted hearts were electrically stimulated, $not3^{+/-}$ hearts exhibited a striking defect in contractility (Figure 5F). Thus, downregulation of *not3* expression in *not3* haploinsufficient mice results in an intrinsic impairment in heart function.

Yeast strains mutant for components of the CCR4-Not complex, including *not3*, display reduced acetylation levels of lysine residues on histone tails (e.g., H3K9) (Peng et al., 2008) and/or reduced trimethylation of H3K4 (Laribee et al., 2007). H3K9 acetylation and H3K4 trimethylation are indicative of transcriptionally active states of chromatin. Moreover, promoter regions of NOT3 target genes were shown to recruit trimethylated H3K4 in mouse ESCs (Hu et al., 2009), suggesting that NOT3 may regulate chromatin modifications. Our gene expression and bioinformatic analyses of mouse *not3* knockout cells revealed that histone deacetylases (HDACs) and mRNA metabolisms are localized central in gene networks (K.K., unpublished data). We therefore assessed the state of histone modifications in hearts from $not3^{+/-}$ mice. Histone extracts of whole hearts from *not3* haploinsufficient mice showed a slight but significant reduction in active histone marks such as acetylation of H3K9 and trimethylation of H3K4 (Figures 5G and 5H and Figure S5). H3K27 trimethylation was not changed (Figure 5I and Figure S5). Treatment of $not3^{+/-}$ hearts with the HDAC inhibitor VPA restored the reduced acetylation of H3K9 and H3K4 trimethylation to that of wild-type levels (Figures 5G–5I and Figure S5). Most importantly, administration of HDAC inhibitors rescued the impairment in heart function in $not3^{+/-}$ mice; i.e., ex vivo heart functions of VPA treated mice were similar to control mice in response to both isoproterenol (Figure 5J) and electrical stimulation (Figure 5K). These data were confirmed with TSA, a second HDAC inhibitor (Figures S5H and S5I). Together, these data show that $not3^{+/-}$ mice exhibit a spontaneous and intrinsic defect in cardiac function that can be rescued with HDAC inhibitors.

$not3^{+/-}$ Mice Develop Severe Cardiomyopathy in Response to Cardiac Stress

We next exposed control and $not3^{+/-}$ littermates to chronic pressure overload by surgical constriction of the aorta (transverse aortic constriction, TAC). Three weeks after TAC, heart weight/body weight ratios (HW/BW) increased in both $not3^{+/+}$ and $not3^{+/-}$ mice, although this increase was significantly larger in the $not3^{+/-}$ mice (Figure 6A). Cardiac hypertrophy was also seen by histology (Figure 6D and Figure S6A). Aortic banding of $not3^{+/-}$ mice resulted in severe heart failure characterized by decreased fractional shortening (Figure 6B) and a dilation of the left ventrical as determined by echocardiography (Figure 6C). In addition, $not3^{+/-}$ mice develop severe cardiac fibrosis after TAC, as shown by Masson-trichrome staining of hearts 3 weeks after TAC (Figure 6D and Figure S6B). Thus, $not3^{+/-}$ mice develop severe symptoms of heart failure in response to cardiac stress.

We next assessed whether HDAC inhibitors can also rescue stress-induced heart failure. HDAC inhibitor treatment could indeed block the augmented loss of cardiac function observed in $not3^{+/-}$ mice after TAC (Figures 7A and 7B). In vivo treatment of $not3^{+/-}$ mice with HDAC inhibitors also blocked the exaggerated induction of heart failure markers such as *ANF* (Figure S6C) and *βMyhc* (Figure S6D). Moreover, treatment with an HDAC inhibitor restored the observed histone alterations in $not3^{+/-}$ mice to that of wild-type littermates (Figure 7C and Figures S6E and S6F). Thus, *not3* haploinsufficiency results in exaggerated heart failure that can be rescued by HDAC inhibition in vivo.

A Common Genomic Variant in the *NOT3* Promoter Correlates with Cardiac Repolarization Duration in Humans

Using an in silico search to identify NOT3 target genes, we found that NOT3 has been shown to bind to the *Kcnq1* promoter in

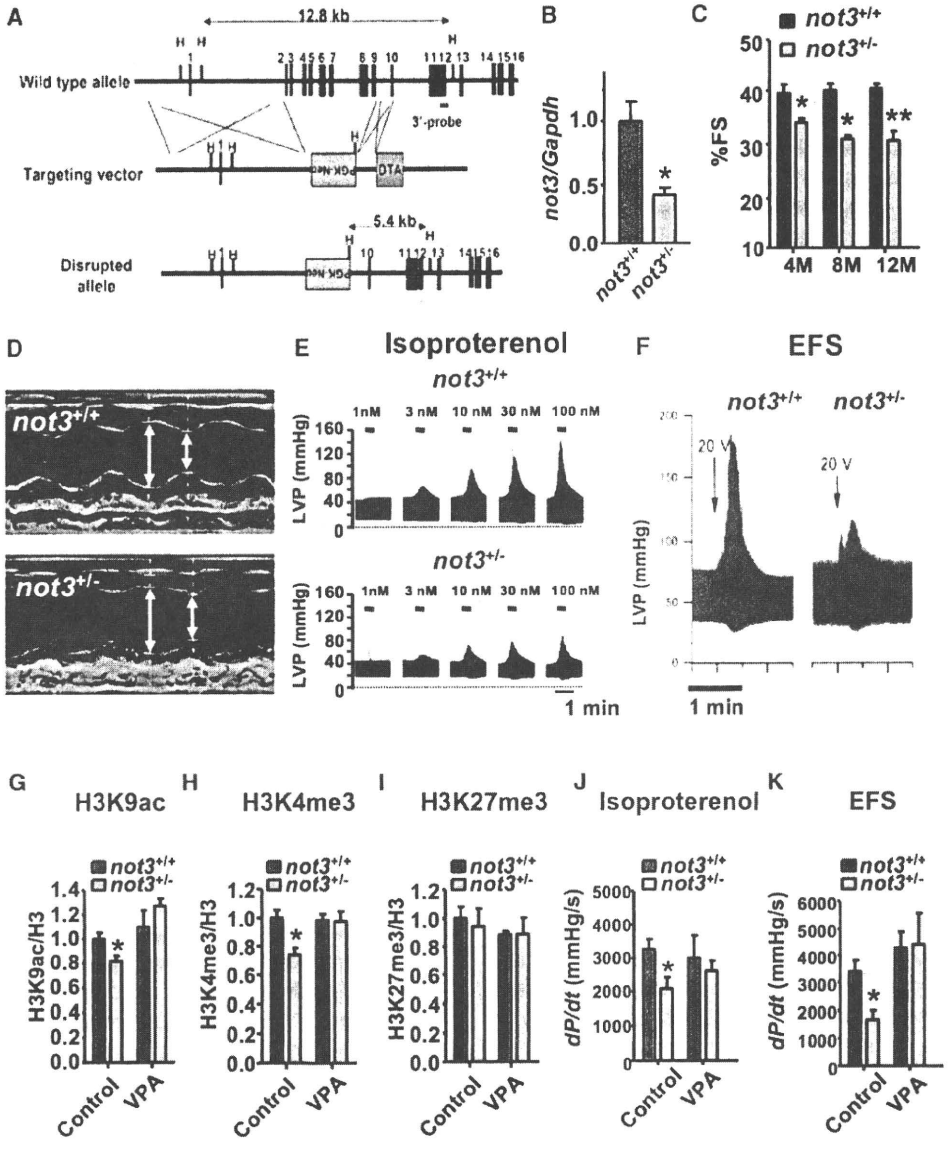

Figure 5. *not3*$^{+/-}$ Mice Exhibit Reduced Heart Contractility, Ex Vivo Function, and Histone Modifications that Can Be Rescued by Treatment with HDAC Inhibitors

(A) Gene targeting strategy. Exons 2 to 9 of the *not3* gene (official symbol *cnot3*) were replaced with a PGK-Neo cassette by homologous recombination in A9 ESCs. The wild-type allele, targeting vector, mutant allele, and PGK-Neo and DTH selection cassettes are shown. Blue boxes indicate exons.

(B) Real-time PCR analyses for *not3* mRNA expression in 3-month-old wild-type and *not3*$^{+/-}$ hearts. Values were normalized to *gapdh* mRNA expression. n = 6 mice per group.

(C) *not3*$^{+/-}$ mice display a significant reduction in percent fractional shortening at 4 months of age, which became more pronounced with age. n = 6–8 mice per group. Fractional shortening was determined by echocardiography.

(D) Representative M mode echocardiography for wild-type and *not3*$^{+/-}$ mice at 8 months of age.

(E) Left ventricular pressure (LVP) measurements in isolated ex vivo *not3*$^{+/-}$ and *not3*$^{+/+}$ hearts under isoproterenol perfusion. *not3*$^{+/-}$ hearts from 4-month-old mice showed impaired contractile responses to different doses of isoproterenol perfusion in the retrograde Langendorff mode as compared to age-matched controls.

(F) Impaired contractile response of ex vivo *not3*$^{+/-}$ hearts to electrical field stimulation (EFS) compared with littermate *not3*$^{+/+}$ hearts. Representative data for left ventricular pressure (LVP) at 20 V stimulation are shown.

(G–I) H3K9 acetylation (H3K9ac) (G), H3K4 trimethylation (H3K4me3) (H), and H3K27 trimethylation (H3K27me3) (I) levels were analyzed by western blot for acid-extracted histones from whole heart ventricles of wild-type and *not3*$^{+/-}$ mice treated with vehicle or VPA (0.71% w/v in drinking water for 1 week) Band intensities were normalized to total H3 levels.

(J and K) Treatment (1 week) with the HDAC inhibitor VPA rescue impaired ex vivo heart contractility of *not3*$^{+/-}$ hearts to isoproterenol (100 nM) perfusion or 25 V EFS.

All values are mean ± SEM. *$p < 0.05$; **$p < 0.01$. n = 5–12 per group. See also Figures S4 and S5.

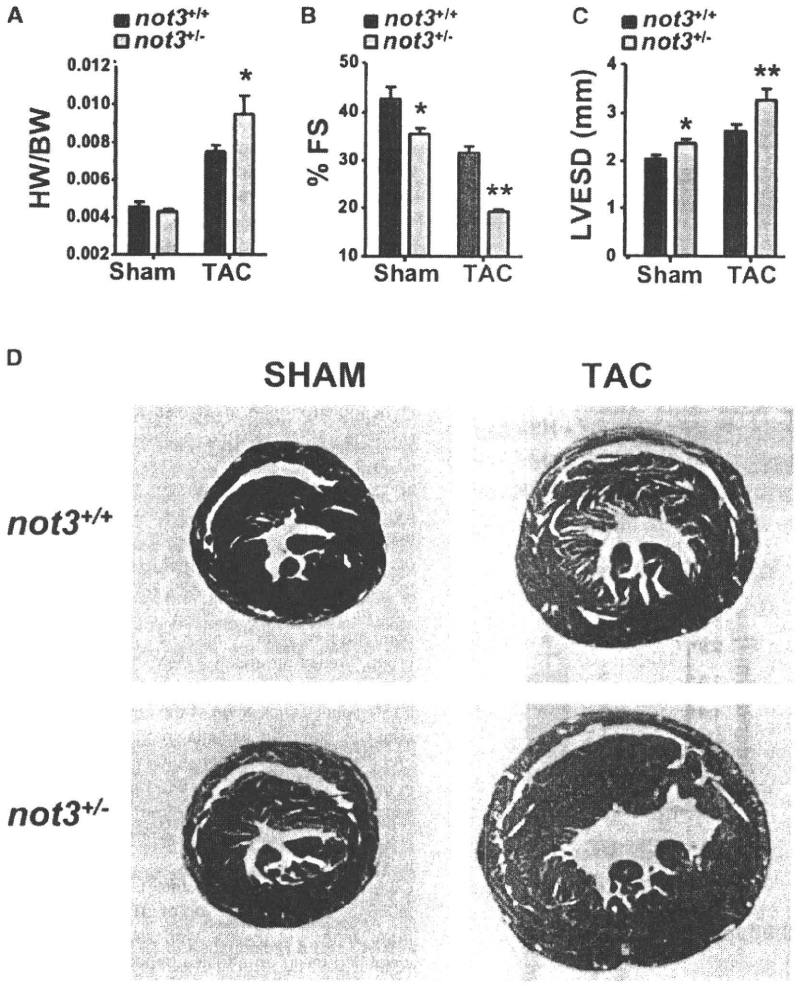

Figure 6. *Not3*$^{+/-}$ Mice Exhibit Severe Heart Failure in Response to Pressure Overload

(A) Heart weight to body weight ratios (HW/BW) in *not3*$^{+/-}$ and *not3*$^{+/+}$ littermate mice 3 weeks after transverse aortic constriction (TAC). Animals receiving sham surgery are shown as controls.

(B and C) Echocardiography of male *not3*$^{+/-}$ and wild-type littermates 3 weeks after TAC. *not3*$^{+/-}$ mice with TAC show decreased percent fractional shortening (%FS) (B) and increased left ventricular diameter in systolic phase (LVESD) (C) compared with *not3*$^{+/+}$ mice that received TAC. All values are mean ± SEM. *$p < 0.05$; **$p < 0.01$.

(D) Representative sections of *not3*$^{+/+}$ and *not3*$^{+/-}$ hearts analyzed 3 weeks after sham or TAC surgery. Masson-trichrome stainings are shown to visualize collagen deposits indicative of fibrotic changes. Note the severe cardiac hypertrophy and ventricular dilation in *not3*$^{+/-}$ mice after TAC.

ESCs (Hu et al., 2009). *Kcnq1* encodes the α subunit of the repolarizing voltage gated potassium channel I_{Ks}, mutations in which are the most common cause of long-QT syndrome (LQT1) in humans (Wang et al., 1996). Abnormalities of cardiac repolarization, measured as alterations in QT interval, predispose to sudden cardiac death in humans (Moss and Kass, 2005). Indeed, while sham-operated *not3*$^{+/-}$ mice exhibit a subtle reduction in cardiac *Kcnq1* expression, this decrease was pronounced after TAC (Figure 7D). Reduced *Kcnq1* expression was rescued after HDAC inhibitor treatment. Also, for *Kcne1*, the β subunit of I_{Ks}, we observed a TAC-inducible and HDAC-sensitive defect in expression in *not3*$^{+/-}$ hearts (Figure 7E). In fly *not3*-RNAi hearts, *KCNQ* expression is also reduced (Figure S3D), and these flies exhibit cardiac contractile irregularities (Figures S3H and S3I).

Recently, two consortia have published genome-wide association studies (GWAS) for QT interval, QT-Interval and Sudden Cardiac Death (QTSCD) (Pfeufer et al., 2009) and Genetics of QT-Interval (QTGEN) (Newton-Cheh et al., 2009). One of the 12 identified genomic regions contains the *NOT1* gene, which we also found as a hit in our *Drosophila* screen (Figures 3A and 3B). Because of the stringent requirements to achieve a genome-wide significance threshold of $p < 5 \times 10^{-8}$ (Dudbridge and Gusnanto, 2008), many genuinely associated alleles will be missed because of both a failure to exceed this statistical threshold and the absence of functional confirmatory data for genes within loci of interest. We therefore evaluated whether common variants in and near the human *NOT3* locus are also associated with alterations in QT interval. Intriguingly, SNP rs36643 (chromosome 19: 59.3 Mb), located in the promoter region ~969 base pairs upstream from the *NOT3* transcriptional start site (924 bases upstream of the TATA box), is significantly associated with QT interval in the QTSCD data set (Figure 7F). Patients carrying the common T allele (minor allele frequency = 0.65) showed a dose-dependent increase in QT interval (ES = +1.03 ± 0.29 ms QT interval per copy of T allele, $p = 3.66E^{-04}$) (Figure 7G). Of note, similar to adult *kcnq1* mutant mice (Nerbonne, 2004), we did not observe an increased QT interval in *not3* heterozygous mice (except for one mouse with arrhythmia, K.K., M.M., H.Y., and K.F., unpublished data). Thus, our genome-wide screening data for death in flies can be used to identify candidate variants in humans that predispose individuals to heart disease, i.e., in the case of *NOT3* to arrhythmia and sudden death.

DISCUSSION

Here, we present the first in vivo RNAi adult heart screen in *Drosophila* assaying conserved genes. Using functional imaging, we were able to observe cardiac defects in all flies with heart-specific knockdown of candidate genes evaluated to date. Our experimental approach to screen for conserved heart genes in *Drosophila* in concert with advanced bioinformatics has the potency to reveal human and mouse genes involved in heart function and heart disease. Moreover, we uncovered a plethora of additional genes, a large proportion of which had

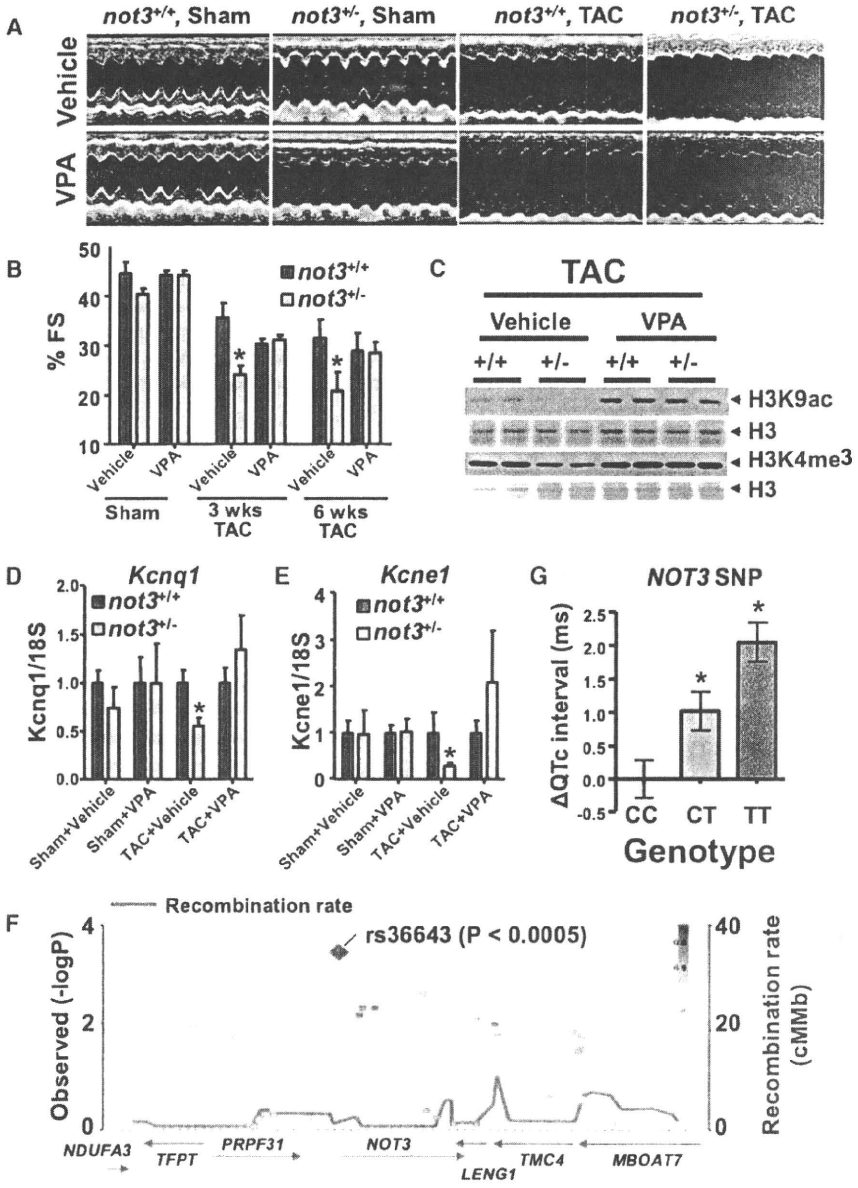

Figure 7. *not3* Is a Conserved Regulator of Heart Function

(A and B) Rescue of severe heart failure in TAC $not3^{+/-}$ hearts by the HDAC inhibitor VPA. One day after TAC or sham surgery, the mice received treatment with vehicle or VPA (0.71% w/v in drinking water) for 6 weeks. Representative M mode echocardiography (A) and percent FS (B) in $not3^{+/-}$ and $not3^{+/+}$ littermate mice 6 weeks after TAC or sham surgery with or without VPA treatment are shown. Values are mean ± SEM. *p < 0.05.

(C) Reduced H3K9 acetylation (H3K9ac) and H3K4 trimethylation (H3K4me3) levels were rescued by VPA treatment. Acid-extracted histones from the hearts 6 weeks after TAC surgery were immunoblotted with antibodies for H3K9ac and H3K4me3. H3 is shown as a loading control.

(D and E) Real-time PCR analyses for the QT interval-associated potassium channel genes *Kcnq1* and *Kcne1*. Total RNA was isolated from hearts 6 weeks after TAC or sham surgery with or without VPA treatment, and *Kcnq1* and *Kcne1* mRNA levels were measured and normalized to *18S* mRNA. Data are shown as fold changes compared to $not3^{+/+}$ mice for each treatment group. Values are mean ± SEM. *p < 0.05; **p < 0.01. n = 5–10 per group.

(F) Regional visualization of the association signal between common variants in the *NOT3* region and the adjusted QT interval (QTc). SNP rs36643 in the 5′ region of *NOT3* (−969 bp from the transcription start and −924 bp from the TATA box) showed a significant regional association (p = 0.000366).

(G) Association between the T allele of SNP rs36643 and a prolongation of QTc. * p < 0.0005 from linear regression with inverse variance weighting using an additive genetic model. Data are derived from a meta-analysis of genome-wide association scans in several populations (Pfeufer et al., 2009).

See also Figure S6.

completely unknown functions until now. Future experiments are required to test whether our candidate genes indeed control cardiac development, regulate adult heart function, and/or influence the outcome of heart failure in response to cardiac stress.

One pathway we identified was the CCR4-Not complex. Functional heart analyses in *Drosophila* confirmed that RNAi-mediated silencing of the CCR4-Not components *not3* and *UBC4* resulted in a severe impairment of cardiac function that resembles dilated cardiomyopathy in experimental mouse models and human patients. To provide a first proof of principle that our fly hits can indeed have similar functions in the more complex mammalian heart, we generated knockout mice for a component of the CCR4-Not complex. *not3* haploinsufficient mice develop spontaneous impairment of heart function and severe heart failure after aortic banding. Mechanistically, *not3* downregulation results in a defect in active histone marks and cardiac defects observed in $not3^{+/-}$ mice could be rescued by treatment with HDAC inhibitors. Besides regulating transcriptionally active states of chromatin (Hu et al., 2009; Jayne et al., 2006; Laribee et al., 2007; Peng et al., 2008), the CCR4-Not complex has also been implicated in RNA deadenylation (Tucker et al., 2001) and microRNA-mediated mRNA degradation (Behm-Ansmant et al., 2006). Thus, we cannot exclude that CCR4-Not components affect additional mechanisms regulating heart function. Importantly, our work on *not3* in flies and mice has also allowed us to identify a single-nucleotide polymorphism in the human *NOT3* promoter that is associated with prolonged QT intervals and sudden cardiac death in humans. Thus, large-scale screens in *Drosophila* can be directly translated to

mammalian species and, in combination with other genome-wide approaches, can reveal regulators of heart function and heart failure.

EXPERIMENTAL PROCEDURES

Detailed experimental procedures are provided in the Extended Experimental Procedures.

Fly Stocks

All RNAi transgenic fly lines were obtained from the Vienna *Drosophila* RNAi Center (VDRC) RNAi stocks (Dietzl et al., 2007). The cardiac tissue-specific *TinCΔ4 12a-Gal4* was a kind gift from Manfred Frasch, (Lo and Frasch, 2001) and *Hand-Gal4* was a gift from Eric Olsen (Han and Olson, 2005).

Screening System

Transgenic RNAi males were crossed to *TinCΔ4* virgin females. Viable lines were then incubated at 29°C for 6 days to expose flies to temperature stress (Paternostro et al., 2001). Initially, a Z score cutoff of 2 (mean control-test)/SD was used to select RNAi lines for retesting.

Drosophila Cardiac Function, Morphology, and Gene Expression

UAS-RNAi fly lines obtained from the Vienna *Drosophila* RNAi Center were crossed to *Hand-Gal4* (II) driver flies and to w^{1118} wild-type control flies. Flies were assessed for heart morphology and physiology with high-speed digital video imaging (Ocorr et al., 2007b). M modes were generated and cardiac parameters including heart periods, diastolic and systolic diameters, and fractional shortening were recorded for each group with a MatLab-based image analysis program (Fink et al., 2009). Fluorescent imaging of *Drosophila* heart tubes was performed as described (Alayari et al., 2009).

Bioinformatics Analysis

For a detailed description of full bioinformatics analysis, please see the Extended Experimental Procedures.

Phenotyping of *not3* Knockout Mice

A targeting vector was constructed to replace exons 2 and 9 of the murine *not3* gene. Fractional shortening (FS) was calculated as follows: FS = [(LVEDD − LVESD)/LVEDD] × 100. For ex vivo heart studies, hearts were assayed with a Langendorff apparatus. The heart was paced electrically at 400 beats/min (bpm), and the electrical field stimulation (EFS) was applied in conjunction with the pacing stimulation. Isoproterenol was perfused for 30 s with the indicated doses. For HDAC inhibition, wild-type and $not3^{+/-}$ mice were treated with vehicle, Trichostatin A (TSA), or Valproic acid (VPA) for 1 week. Acid-extracted histones were prepared, resolved, and transferred to nitrocellulose membranes for western blotting. Transverse aorta constriction (TAC) was performed as described (Kuba et al., 2007). For heart histology, hearts were arrested, fixed, embedded in paraffin, and stained with hematoxylin and eosin (H&E) or Masson-Trichrome.

Human QT Interval Association

Human QT interval association signals over the NOT3 region were obtained from data generated by the QTSCD Consortium (Pfeufer et al., 2009).

SUPPLEMENTAL INFORMATION

Supplemental Information includes Extended Experimental Procedures, six figures, five tables, and one movie and can be found with this article online at doi:10.1016/j.cell.2010.02.023.

ACKNOWLEDGMENTS

We thank all members of our laboratories and the VDRC, the Bioscience Education Research Center (Akita University), and Vincent Chen for helpful discussions and excellent technical support. We thank Eric Olson for the *Hand-Gal4* driver and Manfred Frasch for *TinCΔ4-Gal4* driver stocks. We thank the members of the QTSCD consortium for valuable support and discussion. J.M.P. is supported by the IMBA, the Austrian Ministry of Science, a European Research Council Advanced Investigator grant, and EuGeneHeart. K.K. is supported by Kaken (21659198) from the Japanese Ministry of Science, the Medical Top Track Program, and the Japan Heart Foundation. G.G.N. was supported by a Marie Curie International Incoming Fellowship. A.C. was supported by a postdoctoral fellowship and K.O. by a Scientist Development Grant from the American Heart Association. R.B. was supported by grants from the National Heart, Lung, and Blood Institute of the National Institutes of Health. A.P. is supported by grants 01GR0803 and 01EZ0874 from the German Federal Ministry of Research, FSID-261/2008 from the UK Foundation for the Study of Infant Deaths, and YGEIA/1104/17 and ERYEX/0406/06 from the Cyprus Cardiovascular Disease Educational and Research Trust. Y.I. is supported by the Global Center of Excellence Program.

Received: May 4, 2009
Revised: October 20, 2009
Accepted: February 2, 2010
Published: April 1, 2010

REFERENCES

A.H.A. (2005). http://www.americanheart.org/.

Alayari, N.N., Vogler, G., Taghli-Lamallem, O., Ocorr, K., Bodmer, R., and Cammarato, A. (2009). Fluorescent Labeling of *Drosophila* Heart Structures. J. Vis. Exp. 10.3791/1423.

Albert, T.K., Lemaire, M., van Berkum, N.L., Gentz, R., Collart, M.A., and Timmers, H.T. (2000). Isolation and characterization of human orthologs of yeast CCR4-NOT complex subunits. Nucleic Acids Res. *28*, 809–817.

Behm-Ansmant, I., Rehwinkel, J., Doerks, T., Stark, A., Bork, P., and Izaurralde, E. (2006). mRNA degradation by miRNAs and GW182 requires both CCR4:NOT deadenylase and DCP1:DCP2 decapping complexes. Genes Dev. *20*, 1885–1898.

Bodmer, R. (1995). Heart development in Drosophila and its relationship to vertebrates. Trends Cardiovasc. Med. *5*, 21–28.

Cripps, R.M., and Olson, E.N. (2002). Control of cardiac development by an evolutionarily conserved transcriptional network. Dev. Biol. *246*, 14–28.

Denis, C.L. (1984). Identification of new genes involved in the regulation of yeast alcohol dehydrogenase II. Genetics *108*, 833–844.

Dietzl, G., Chen, D., Schnorrer, F., Su, K.C., Barinova, Y., Fellner, M., Gasser, B., Kinsey, K., Oppel, S., Scheiblauer, S., et al. (2007). A genome-wide transgenic RNAi library for conditional gene inactivation in Drosophila. Nature *448*, 151–156.

Dudbridge, F., and Gusnanto, A. (2008). Estimation of significance thresholds for genomewide association scans. Genet. Epidemiol. *32*, 227–234.

Fink, M., Callol-Massot, C., Chu, A., Ruiz-Lozano, P., Izpisua Belmonte, J.C., Giles, W., Bodmer, R., and Ocorr, K. (2009). A new method for detection and quantification of heartbeat parameters in Drosophila, zebrafish, and embryonic mouse hearts. Biotechniques *46*, 101–113.

Gordon, T., Castelli, W.P., Hjortland, M.C., Kannel, W.B., and Dawber, T.R. (1977). Predicting coronary heart disease in middle-aged and older persons. The Framington study. JAMA *238*, 497–499.

Han, Z., and Olson, E.N. (2005). Hand is a direct target of Tinman and GATA factors during Drosophila cardiogenesis and hematopoiesis. Development *132*, 3525–3536.

Hu, G., Kim, J., Xu, Q., Leng, Y., Orkin, S.H., and Elledge, S.J. (2009). A genome-wide RNAi screen identifies a new transcriptional module required for self-renewal. Genes Dev. *23*, 837–848.

Jayne, S., Zwartjes, C.G., van Schaik, F.M., and Timmers, H.T. (2006). Involvement of the SMRT/NCoR-HDAC3 complex in transcriptional repression by the CNOT2 subunit of the human Ccr4-Not complex. Biochem. J. *398*, 461–467.

Joza, N., Oudit, G.Y., Brown, D., Bénit, P., Kassiri, Z., Vahsen, N., Benoit, L., Patel, M.M., Nowikovsky, K., Vassault, A., et al. (2005). Muscle-specific

loss of apoptosis-inducing factor leads to mitochondrial dysfunction, skeletal muscle atrophy, and dilated cardiomyopathy. Mol. Cell. Biol. *25*, 10261–10272.

Kuba, K., Zhang, L., Imai, Y., Arab, S., Chen, M., Maekawa, Y., Leschnik, M., Leibbrandt, A., Markovic, M., Makovic, M., et al. (2007). Impaired heart contractility in Apelin gene-deficient mice associated with aging and pressure overload. Circ. Res. *101*, e32–e42.

Lakatta, E.G., and Levy, D. (2003). Arterial and cardiac aging: major shareholders in cardiovascular disease enterprises: Part II: the aging heart in health: links to heart disease. Circulation *107*, 346–354.

Laribee, R.N., Shibata, Y., Mersman, D.P., Collins, S.R., Kemmeren, P., Roguev, A., Weissman, J.S., Briggs, S.D., Krogan, N.J., and Strahl, B.D. (2007). CCR4/NOT complex associates with the proteasome and regulates histone methylation. Proc. Natl. Acad. Sci. USA *104*, 5836–5841.

Lloyd-Jones, D., Adams, R., Carnethon, M., De Simone, G., Ferguson, T.B., Flegal, K., Ford, E., Furie, K., Go, A., Greenlund, K., et al. American Heart Association Statistics Committee and Stroke Statistics Subcommittee. (2009). Heart disease and stroke statistics—2009 update: a report from the American Heart Association Statistics Committee and Stroke Statistics Subcommittee. Circulation *119*, e21–e181.

Lo, P.C., and Frasch, M. (2001). A role for the COUP-TF-related gene seven-up in the diversification of cardioblast identities in the dorsal vessel of Drosophila. Mech. Dev. *104*, 49–60.

Morita, H., Seidman, J., and Seidman, C.E. (2005). Genetic causes of human heart failure. J. Clin. Invest. *115*, 518–526.

Moss, A.J., and Kass, R.S. (2005). Long QT syndrome: from channels to cardiac arrhythmias. J. Clin. Invest. *115*, 2018–2024.

Mudd, J.O., and Kass, D.A. (2008). Tackling heart failure in the twenty-first century. Nature *451*, 919–928.

Nabel, E.G. (2003). Cardiovascular disease. N. Engl. J. Med. *349*, 60–72.

Nerbonne, J.M. (2004). Studying cardiac arrhythmias in the mouse—a reasonable model for probing mechanisms? Trends Cardiovasc. Med. *14*, 83–93.

Newton-Cheh, C., Eijgelsheim, M., Rice, K.M., de Bakker, P.I., Yin, X., Estrada, K., Bis, J.C., Marciante, K., Rivadeneira, F., Noseworthy, P.A., et al. (2009). Common variants at ten loci influence QT interval duration in the QTGEN Study. Nature genetics *41*, 399–406.

Ocorr, K., Perrin, L., Lim, H.Y., Qian, L., Wu, X., and Bodmer, R. (2007a). Genetic control of heart function and aging in Drosophila. Trends Cardiovasc. Med. *17*, 177–182.

Ocorr, K., Reeves, N.L., Wessells, R.J., Fink, M., Chen, H.S., Akasaka, T., Yasuda, S., Metzger, J.M., Giles, W., Posakony, J.W., and Bodmer, R. (2007b). KCNQ potassium channel mutations cause cardiac arrhythmias in Drosophila that mimic the effects of aging. Proc. Natl. Acad. Sci. USA *104*, 3943–3948.

Paternostro, G., Vignola, C., Bartsch, D.U., Omens, J.H., McCulloch, A.D., and Reed, J.C. (2001). Age-associated cardiac dysfunction in Drosophila melanogaster. Circ. Res. *88*, 1053–1058.

Peng, W., Togawa, C., Zhang, K., and Kurdistani, S.K. (2008). Regulators of cellular levels of histone acetylation in Saccharomyces cerevisiae. Genetics *179*, 277–289.

Pfeufer, A., Sanna, S., Arking, D.E., Müller, M., Gateva, V., Fuchsberger, C., Ehret, G.B., Orrú, M., Pattaro, C., Köttgen, A., et al. (2009). Common variants at ten loci modulate the QT interval duration in the QTSCD Study. Nat. Genet. *41*, 407–414.

Qian, L., and Bodmer, R. (2009). Partial loss of GATA factor Pannier impairs adult heart function in Drosophila. Hum. Mol. Genet. *18*, 3153–3163.

Qian, L., Mohapatra, B., Akasaka, T., Liu, J., Ocorr, K., Towbin, J.A., and Bodmer, R. (2008). Transcription factor neuromancer/TBX20 is required for cardiac function in Drosophila with implications for human heart disease. Proc. Natl. Acad. Sci. USA *105*, 19833–19838.

Ray, V.M., and Dowse, H.B. (2005). Mutations in and deletions of the Ca2+ channel-encoding gene cacophony, which affect courtship song in Drosophila, have novel effects on heartbeating. J. Neurogenet. *19*, 39–56.

Rusconi, J.C., and Challa, U. (2007). Drosophila Mrityu encodes a BTB/POZ domain-containing protein and is expressed dynamically during development. Int. J. Dev. Biol. *51*, 259–263.

Sanguinetti, M.C., and Tristani-Firouzi, M. (2006). hERG potassium channels and cardiac arrhythmia. Nature *440*, 463–469.

Sanyal, S., Jennings, T., Dowse, H., and Ramaswami, M. (2006). Conditional mutations in SERCA, the Sarco-endoplasmic reticulum Ca2+-ATPase, alter heart rate and rhythmicity in Drosophila. J. Comp. Physiol. [B] *176*, 253–263.

Tucker, M., Valencia-Sanchez, M.A., Staples, R.R., Chen, J., Denis, C.L., and Parker, R. (2001). The transcription factor associated Ccr4 and Caf1 proteins are components of the major cytoplasmic mRNA deadenylase in Saccharomyces cerevisiae. Cell *104*, 377–386.

Wang, Q., Curran, M.E., Splawski, I., Burn, T.C., Millholland, J.M., VanRaay, T.J., Shen, J., Timothy, K.W., Vincent, G.M., de Jager, T., et al. (1996). Positional cloning of a novel potassium channel gene: KVLQT1 mutations cause cardiac arrhythmias. Nat. Genet. *12*, 17–23.

Yusuf, S., Reddy, S., Ounpuu, S., and Anand, S. (2001). Global burden of cardiovascular diseases: part I: general considerations, the epidemiologic transition, risk factors, and impact of urbanization. Circulation *104*, 2746–2753.

Oncogene (2010) 29, 2070–2082

www.nature.com/onc

ORIGINAL ARTICLE

Involvement of JNK in the regulation of autophagic cell death

S Shimizu[1,2], A Konishi[3], Y Nishida[1,2], T Mizuta[2], H Nishina[4], A Yamamoto[5] and Y Tsujimoto[1]

[1]Department of Medical Genetics, Osaka University Medical School, Yamada-oka, Suita, Osaka, Japan; [2]Department of Pathological Cell Biology, Medical Research Institute, Tokyo Medical and Dental University, Yushima, Bunkyo-ku, Tokyo, Japan; [3]Medical Top Track Program, Medical Research Institute, Tokyo Medical and Dental University, Yushima, Bunkyo-ku, Tokyo, Japan; [4]Department of Developmental and Regenerative Biology, Medical Research Institute, Tokyo Medical and Dental University, Yushima, Bunkyo-ku, Tokyo, Japan and [5]Department of Bio-Science, Nagahama Institute of Bio-Science and Technology, Nagahama, Japan

Programmed cell death is a crucial process in the normal development and physiology of metazoans, and it can be divided into several categories that include type I death (apoptosis) and type II death (autophagic cell death). The Bcl-2 family proteins are well-characterized regulators of apoptosis, among which multidomain pro-apoptotic members (such as Bax and Bak) function as a mitochondrial gateway at which various apoptotic signals converge. Although embryonic fibroblasts from Bax/Bak double-knockout (DKO) mice are resistant to apoptosis, we have previously reported that these cells still die by autophagy in response to various death stimuli. In this study, we found that jun N-terminal kinase (JNK) was activated in etoposide- and staurosporine-treated, but not serum-starved, Bax/Bak DKO cells, and that autophagic cell death was suppressed by the addition of a JNK inhibitor and by a dominant-negative mutant of JNK. Studies with sek1$^{-/-}$mkk7$^{-/-}$ cells revealed that disruption of JNK prevented the induction of autophagic cell death. Co-activation of JNK and autophagy induced autophagic cell death. Activation of JNK occurred downstream of the induction of autophagy, and was dependent on the autophagic process. These results indicate that JNK activation is crucial for the autophagic death of Bax/Bak DKO cells.
Oncogene (2010) **29,** 2070–2082; doi:10.1038/onc.2009.487; published online 18 January 2010

Keywords: JNK; autophagic cell death; Atg5

Introduction

Programmed cell death is a genetically regulated mechanism of cell death, which is essential for various biological events, such as morphogenesis and the elimination of potentially harmful cells. Apoptosis is a representative form of programmed cell death, which is regulated by the Bcl-2 family proteins and driven by a family of cysteine proteases called caspases, which have already been intensively investigated. In addition, accumulating evidence suggests that other mechanisms may also contribute to programmed cell death. One of these non-apoptotic death mechanisms may be the so-called 'autophagic cell death' or type II programmed cell death, which is morphologically defined as deaths of cells associated with autophagic changes (Clarke, 1990; Bachrecke, 2002).

Autophagy is an evolutionarily conserved process, which operates constitutively to allow bulk degradation of cellular constituents and organelles in healthy cells, and it is induced above basal levels in response to various stimuli that include starvation, genotoxic stress and deprivation of cytokines (Ohsumi, 2001; Mizushima *et al.*, 2002; Klinonsky, 2005). During the process of autophagy, cellular cytoplasm and organelles are engulfed by double-membrane vesicles called autophagosomes that fuse with lysosomes to become autolysosomes, in which the cargo of the autophagosomes are degraded by lysosomal enzymes. Studies performed in yeasts have revealed more than 30 molecules that are involved in autophagy, including Atg5 and Atg6 (also called Beclin 1), and homologues for these molecules have been found in mammals, providing us with clues to study the physiological process of autophagy (Ohsumi, 2001; Mizushima *et al.*, 2002; Klinonsky, 2005).

Autophagy is primarily a pro-survival mechanism, but there is evidence to suggest that it also functions as a pro-death mechanism under certain conditions (Levine and Yuan, 2005). We previously discovered that embryonic fibroblasts from Bax/Bak double-knockout (DKO) mice are resistant to apoptosis, but still die in a non-apoptotic manner with autophagic features after death stimulation (Shimizu *et al.*, 2004). We have also shown that such non-apoptotic death of Bax/Bak DKO cells is suppressed by inhibitors of autophagy, including a type III phosphoinositide-3 kinase inhibitor, 3-methyl adenine (3-MA), and is dependent on autophagic proteins, such as Atg5 and Beclin 1, indicating that this form of cell death occurs through autophagic machinery (Shimizu *et al.*, 2004). Similarly, Lenardo and colleagues

Correspondence: Professor S Shimizu or Professor Y Tsujimoto, Department of Pathological Cell Biology, Medical Research Institute, Tokyo Medical and Dental University, Yushima, 1-5-45, Bunkyo-ku, Tokyo 103-5802, Japan, or Department of Medical Genetics, Osaka University Medical School, 2-2 Yamadaoka, Suita, Osaka 565-0871, Japan.
E-mails: shimizu.pcb@mri.tmd.ac.jp or tsujimot@gene.med.osaka-u.ac.jp
Received 22 July 2009; revised 17 November 2009; accepted 7 December 2009; published online 18 January 2010

have demonstrated the induction of autophagic cell death when L929 cells were treated with benzyloxycarbonyl-Val-Ala-Asp (OMe) fluoromethylketone (zVAD-fmk), a broad-spectrum caspase inhibitor (Yu *et al.*, 2004). Similar to etoposide-treated Bax/Bak DKO mouse embryonic fibroblasts (MEFs), zVAD-fmk-treated L929 cells die of autophagy, and this form of cell death is blocked by silencing of Atg7 and Beclin 1 (Yu *et al.*, 2004). In both cases, molecules involved in autophagy apparently promote cell death rather than cell survival. When cells are starved, death eventually occurs because of autophagy, but it does not depend on autophagic proteins. Therefore, there are two kinds of autophagy-related cell death, with one being dependent on autophagy and the other being death that is not driven by autophagy. To understand the physiological and pathological roles of autophagic cell death, particularly the autophagy-dependent form of death, it is necessary to elucidate how autophagic molecules are involved in cellular destruction and to find the other molecules that also have a role in this form of cell death. Accordingly, we searched for molecules that were involved in the autophagic death of Bax/Bak DKO MEFs. As a result, we demonstrated that activation of jun N-terminal kinase (JNK) was required for the autophagic death of these cells and that such activation occurred downstream of the autophagic process itself.

Results

Phosphorylation of JNK during etoposide-induced and staurosporine-induced autophagic death of Bax/Bak DKO MEFs

Recently, we showed that various apoptotic stimuli, including etoposide and staurosporine, were able to induce the autophagic death of Bax/Bak DKO MEFs (Shimizu *et al.*, 2004), in which mitochondria-mediated apoptosis signaling is blocked. However, detailed mechanisms underlying this form of cell death were unclear. As JNK was reported to have a crucial role in inducing the autophagic death of zVAD-fmk-treated L929 cells (Yu *et al.*, 2004), we assumed that JNK might act as a pivotal signaling molecule for etoposide (or staurosporine)-induced autophagic death of Bax/Bak DKO MEFs. As shown in Figure 1, the activation of JNK was detected in etoposide-treated Bax/Bak DKO MEFs by the *in vitro* kinase assay (Figure 1a) and by western blot analysis of phospho-JNK (Figure 1b). Addition of SP600125, a JNK inhibitor, prevented the phosphorylation of JNK (Figure 1b). Similar results were obtained with staurosporine (Figure1a; data not shown). Although phosphorylated/active JNK showed molecular sizes of both 46 and 54 kD on western blotting, the 46-kD phosphorylated JNK was dominant in etoposide-treated and staurosporine-treated Bax/Bak DKO MEFs (Figure1b; data not shown). Etoposide caused immediate and sustained activation of JNK with a peak after 3–4 h. Sustained activation of JNK is reported to be linked with cell death (Ventura *et al.*, 2006). Unlike JNK, we did not detect activation of other stress-related mitogen-activated protein kinases, such as p38, extracellular ligand-regulated kinase (ERK)1/2 and ERK5 (Figures 1c–e). These results indicated that JNK was activated in Bax/Bak DKO MEFs by etoposide or staurosporine treatment.

Involvement of JNK in etoposide-induced and staurosporine-induced autophagic death of Bax/Bak DKO MEFs

As JNK was activated in etoposide-treated and staurosporine-treated Bax/Bak DKO MEFs, we next investigated whether its activation was required for etoposide-induced and staurosporine-induced death of Bax/Bak DKO MEFs. As shown in Figure 2a, etoposide-treated Bax/Bak DKO MEFs became rounded and detached from the culture dish, consistent with our previous findings (Shimizu *et al.*, 2004). These cells showed loss of viability when assessed by staining with propidium iodide (PI; a membrane-impermeable stain for nucleic acid staining; Figures 2b and c), as well as by the colony formation assay (Figure 2d) and the cell growth assay using Cell Titer Blue (CTB) to measure the metabolic activity of viable cells (Figure 2e). When Bax/Bak DKO MEFs were treated with etoposide in the presence of 3-MA (an inhibitor of autophagy through type III phosphoinositide-3 kinase), both morphological changes and cell viability were markedly improved (Figures 2a–e), which was also consistent with our previous observations (Shimizu *et al.*, 2004). When SP600125 was added instead of 3-MA, cell rounding and detachment were inhibited, but to lesser extent than with 3-MA (Figure 2a). Similarly, cell viability (assessed by PI staining, colony formation and cell growth) was improved by the addition of JNK inhibitor in a dose-dependent manner, but to a lesser extent than that caused by the addition of 3-MA (Figures 2b–e). Similar results were obtained with staurosporine (Figure 2f). In contrast, a p38 inhibitor (SB203580) and an ERK1/2 inhibitor (U0126) did not have any influence on the extent of autophagic cell death (Figure 2c), a finding consistent with the lack of p38 activation and ERK1/2 activation by etoposide (Figures 1c and d).

For further confirmation of the role of JNK, a dominant-negative form of JNK was expressed in Bax/Bak DKO MEFs to specifically inhibit JNK activation (Figure 2g). As shown in Figures 2h and i, etoposide-induced autophagic death of Bax/Bak DKO MEFs was significantly suppressed by transfection with the dominant-negative JNK plasmid, but not the empty vector, as assessed by PI staining and the CTB assay, confirming the involvement of JNK in autophagic cell death.

To investigate the involvement of JNK in autophagic cell death from another perspective, we used a genetic approach. Activation of JNK requires phosphorylation of both tyrosine (^{185}Tyr) and threonine (^{183}Thr), and two kinases (SEK1 (also known as MKK4) and MKK7 (SEK2)) are essential for the phosphorylation of these amino-acid residues. Therefore, JNK activation is completely abolished in sek1$^{-/-}$ mkk7$^{-/-}$ cells (Nishitai *et al.*, 2004). As we previously demonstrated that, similar to Bax/Bak DKO MEFs, MEFs overexpressing

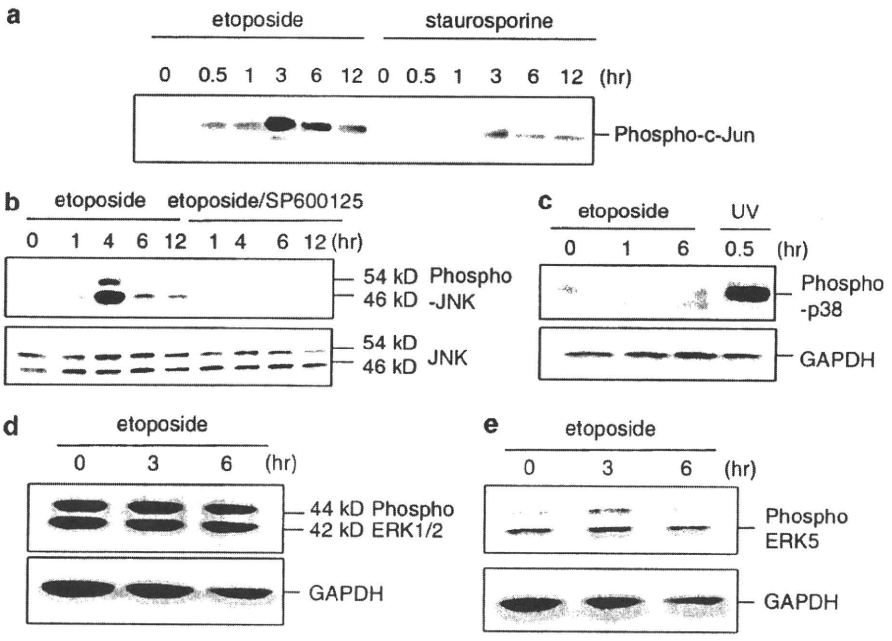

Figure 1 Phosphorylation of jun N-terminal kinase (JNK) after treatment of Bax/Bak double-knockout (DKO) mouse embryonic fibroblasts (MEFs) with etoposide or staurosporine. (**a**) DKO MEFs were treated with 20 μM etoposide or 1 μM staurosporine (STS) for the indicated periods. Cell lysates were subjected to an *in vitro* c-Jun kinase assay using an anti-phosphorylated c-Jun antibody. (**b**, **c**) DKO MEFs were treated with 20 μM etoposide or ultraviolet (UV) irradiation (100 J/m^2) in the presence or absence of 25 μM SP600125 for the indicated periods. Cell lysates were then subjected to immunoblot analysis with antibodies for phosphorylated JNK, JNK, phosphorylated p38 or glyceraldehyde 3-phosphate dehydrogenase (GAPDH; loading control). UV irradiation was used as a positive control for p38 activation. (**d**, **e**) DKO MEFs were treated with 20 μM etoposide for the indicated periods. Cell lysates were then subjected to immunoblot analysis with antibodies against phosphorylated extracellular ligand-regulated kinase (ERK)1/2, phosphorylated ERK5 or GAPDH (loading control).

Bcl-x_L die through an autophagic process after etoposide or staurosporine treatment (Shimizu *et al.*, 2004), Bcl-x_L was expressed in wild-type (WT) and sek1$^{-/-}$ mkk7$^{-/-}$ cells that were treated with etoposide. The WT cells overexpressing Bcl-x_L showed resistance to etoposide-induced cell death compared with vector-transfected WT MEFs, but still had a significant decline of viability, which was suppressed by the addition of 3-MA (Figure 3a). In contrast, the viability of Bcl-x_L-expressing sek1$^{-/-}$ mkk7$^{-/-}$ cells was higher than that of Bcl-x_L-expressing WT cells and was not influenced by the addition of 3-MA (Figure 3b). In both types of cells, the level of Bcl-x_L expression was equivalent and apoptosis was similarly inhibited (Figure 3c; data not shown). Therefore, 3-MA-sensitive autophagic cell death was blocked in Bcl-x_L-expressing sek1$^{-/-}$ mkk7$^{-/-}$ cells. Note that autophagy was activated similarly in both WT and sek1$^{-/-}$ mkk7$^{-/-}$ cells (Figure 3d). Consistent with the above findings, inhibition of autophagy using small interfering RNA (siRNA) for Atg5, which is essential for the induction of autophagy, improved the viability of Bcl-x_L-overexpressing WT cells, but not of Bcl-x_L-overexpressing sek1$^{-/-}$ mkk7$^{-/-}$ cells (Figures 3e and f). Thus, 3-MA-sensitive and Atg5-dependent autophagic cell death was induced in Bcl-x_L-overexpressing WT cells, but not in Bcl-x_L-overexpressing sek1$^{-/-}$ mkk7$^{-/-}$ cells, indicating that activation of JNK was required for the induction of autophagic cell death, consistent with the data shown in Figure 2.

JNK is activated during autophagic cell death, but not during starvation-induced autophagy

Autophagy occurs during autophagic cell death, but is also induced by starvation of cells. We have already demonstrated that JNK is activated during autophagic cell death. We next investigated whether starvation-induced autophagy was also accompanied by the activation of JNK. When Bax/Bak DKO MEFs were starved by incubation in Hanks solution, as described in Materials and methods section, autophagy occurred, as demonstrated by the punctate distribution of green fluorescent protein (GFP)-tagged light chain 3 (LC3; Figure 4a). As shown in Figure 4b, kinetics of autophagy induction were different between etoposide-treated cells and starved cells. Unlike etoposide treatment, starvation did not induce cell death (Figure 4c). As would be expected if it were assumed that autophagy was activated to promote survival during starvation, the death of these cells was enhanced by 3-MA (Figure 4c). In these cells, the level of JNK activation remained low compared with that in etoposide-treated cells (Figure 4d), suggesting that activation of JNK occurred with the induction of autophagic cell death but not autophagy for survival.

Co-activation of JNK and autophagy is sufficient to induce autophagic death of Bax/Bak DKO MEFs

Having shown that JNK has a crucial role in autophagic cell death, we next investigated whether JNK activation

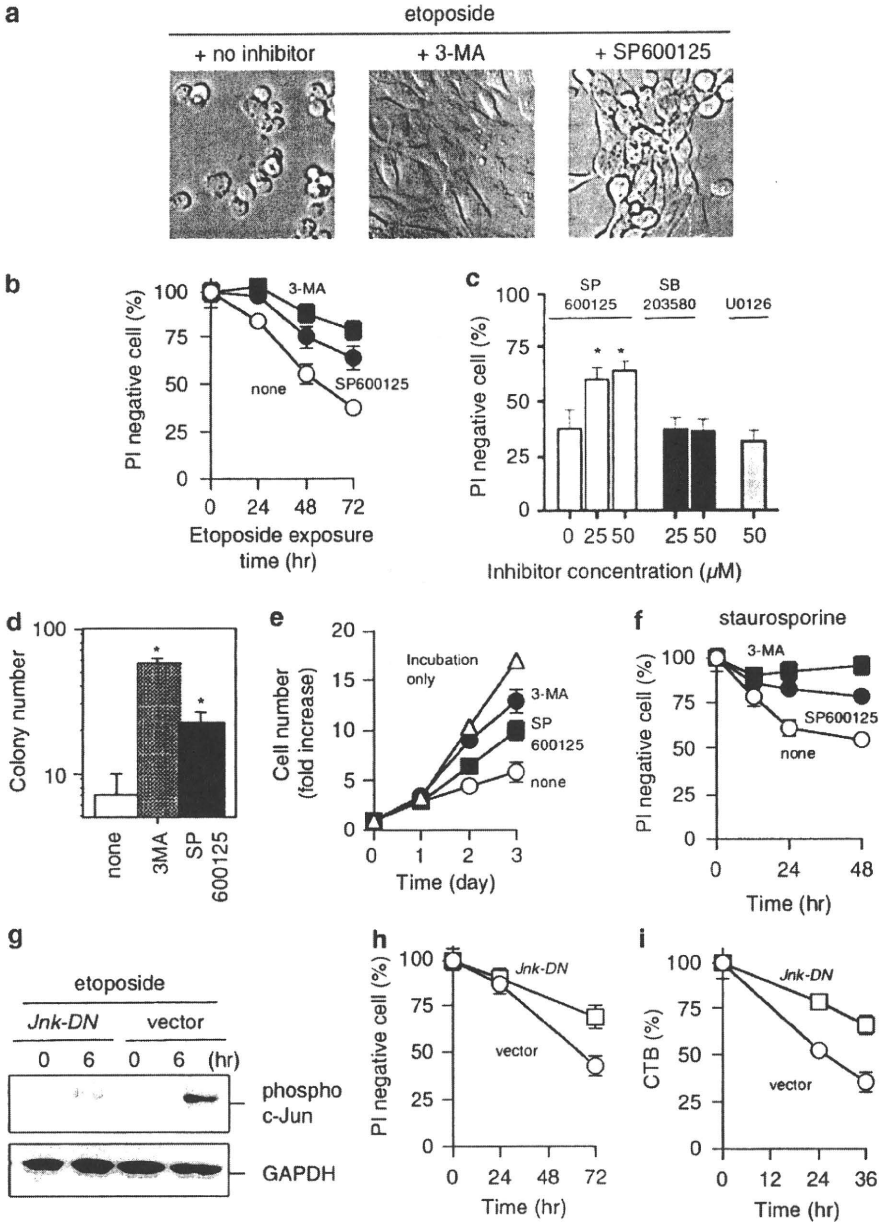

Figure 2 Reduction of etoposide-induced and staurosporine-induced death in Bax/Bak double-knockout (DKO) mouse embryonic fibroblasts (MEFs) by inhibition of jun N-terminal kinase (JNK). (**a**) DKO MEFs were treated with etoposide (20 μM) in the absence or presence of 10 mM 3-MA or 25 μM SP600125 for 24 h, and then were examined by phase-contrast microscopy. (**b**, **c**) Reduction of etoposide-induced autophagic cell death by SP600125 and 3-MA, but not SB203580 and U0126 as assessed by PI staining. (**b**) DKO MEFs were treated with 20 μM etoposide in the absence (open circles) or presence of 10 mM 3-MA (closed squares) or 25 μM SP600125 (closed circles) for the indicated periods. (**c**) DKO MEFs were treated with 20 μM etoposide in the presence of the indicated concentrations of SP600125, SB203580, or U0126 for 72 h. Cell viability was measured by staining with PI. Asterisks indicate a significant difference at $P<0.05$ (vs no inhibitor). (**d**, **e**) Reduction of etoposide-induced death by SP600125, as assessed by the clonogenic and proliferation assays. (**d**) DKO MEFs were treated with 20 μM etoposide in the absence or presence of 10 mM 3-methyl adenine (3-MA) or 25 μM SP600125 for 24 h. After collection, 2000 cells were seeded in normal medium and the number of colonies was counted after 1 week. Asterisks indicate a significant difference at $P<0.05$ (vs none). (**e**) DKO MEFs were untreated (open triangles) or treated with 20 μM etoposide in the absence (open circles) or presence of 10 mM 3-MA (closed circles) or 25 μM SP600125 (closed squares) for 24 h, and 5000 cells were seeded in normal medium. The number of viable cells was measured on the indicated days by the Cell Titer Blue (CTB) assay. (**f**) Reduction of staurosporine-induced autophagic cell death by SP600125 and 3-MA, as assessed by propidium iodide (PI) staining. DKO MEFs were treated with 1 μM staurosporine in the absence (open circles) or presence of 10 mM 3-MA (closed squares) or 25 μM SP600125 (closed circles) for the indicated periods. Cell viability was measured by PI staining. (**g**–**i**) Reduction of etoposide-induced autophagic cell death by a dominant-negative JNK mutation. DKO MEFs were transfected with plasmid DNA for the dominant-negative JNK mutation or the empty vector. After 24 h, cells were incubated with 20 μM etoposide for the indicated periods. Activation of JNK was assessed by the immunoblot analysis with antibodies for phsphorylated c-Jun (**g**). Cell viability was assessed by the PI staining (**h**) and CTB assay (**i**). In panels **b**–**f**, **h** and **i**, data are expressed as mean ± s.d. for four independent experiments.

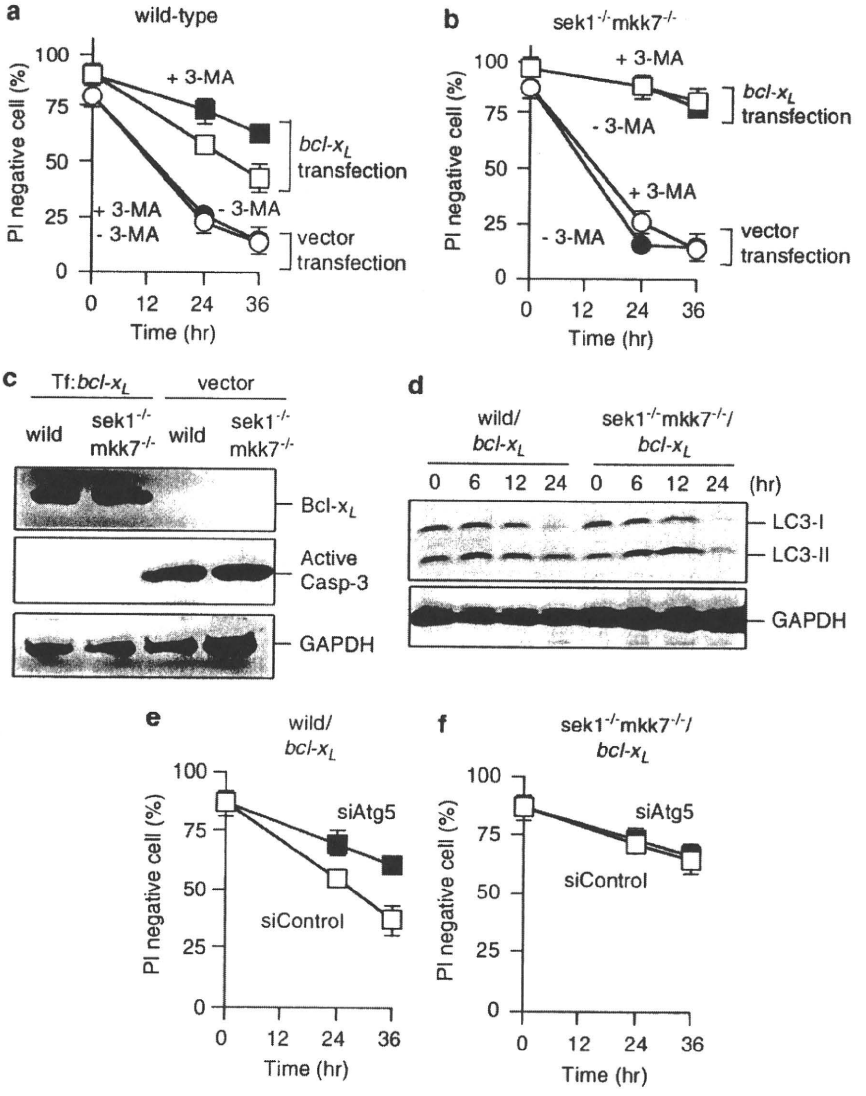

Figure 3 Suppression of etoposide-induced autophagic death in Bcl-x_L-overexpressing sek1 $^{-/-}$ mkk7 $^{-/-}$ mouse embryonic fibroblast (MEF)-like cells. (**a**, **b**) Wild-type (**a**) and sek1 $^{-/-}$ mkk7 $^{-/-}$ (**b**) MEF-like cells were transfected with plasmid DNA for Bcl-x_L (squares) or the empty vector (circles) for 24 h, and then were incubated with 20 μM etoposide in the presence (closed) or absence (open) of 10 mM 3-methyl adenine (3-MA) for the indicated periods. Cell viability was assessed by propidium iodide (PI) staining. Data are expressed as mean ± s.d. for four independent experiments. (**c**, **d**) Wild-type and sek1 $^{-/-}$ mkk7 $^{-/-}$ MEF-like cells were transfected with plasmid DNA for Bcl-x_L or the empty vector, and then were incubated with 20 μM etoposide for 18 h (**c**) or for the indicated periods (**d**). Cell lysates were then subjected to immunoblot analysis with antibodies against Bcl-x_L or active caspases 3 (**c**) or light chain 3 (LC3) (**d**). Glyceraldehyde 3-phosphate dehydrogenase (GAPDH) is used as the loading control. (**e**, **f**) Wild-type (**e**) and sek1 $^{-/-}$ mkk7 $^{-/-}$ (**f**) MEF-like cells were transfected with the Bcl-x_L expression plasmid together with Atg5 small interfering RNA (siRNA; closed squares) or control siRNA (open squares), and were incubated with 20 μM etoposide for the indicated periods. Cell viability was assessed by PI staining. Data are expressed as mean ± s.d. for four independent experiments.

was sufficient to induce autophagic cell death by using an MKK7–JNK fusion protein, in which MKK7α1 and JNK1β1 were connected by the Flag tag (Tsuruta *et al.*, 2004). Expression of this fusion protein led to constitutive activation of JNK through intramolecular phosphorylation by MKK7 (Figure 5a). As shown in Figure 5b, transient expression of MKK7–JNK in WT MEFs induced death, which was inhibited by zVAD-fmk. These findings indicated that WT MEFs underwent apoptosis due to autoactivation of JNK, consistent with numerous previous reports (Gupta *et al.*, 1995), thus verifying that MKK7–JNK functioned properly in our transfected cells. The addition of 3-MA enhanced this apoptosis, consistent with other report demonstrating that inhibition of autophagy enhances apoptosis (Boya *et al.*, 2005). We then introduced this plasmid into DKO MEFs. If activation of JNK was sufficient to induce autophagic cell death, expression of MKK7–JNK should have induced the death of Bax/Bak DKO MEFs. However, despite the similar level of JNK activation in WT and DKO MEFs (Figure 5a), expression of the MKK7–JNK fusion protein did not induce the death in Bax/Bak DKO MEFs (Figure 5b), indicating that activation of JNK alone was not sufficient to cause autophagic cell death.

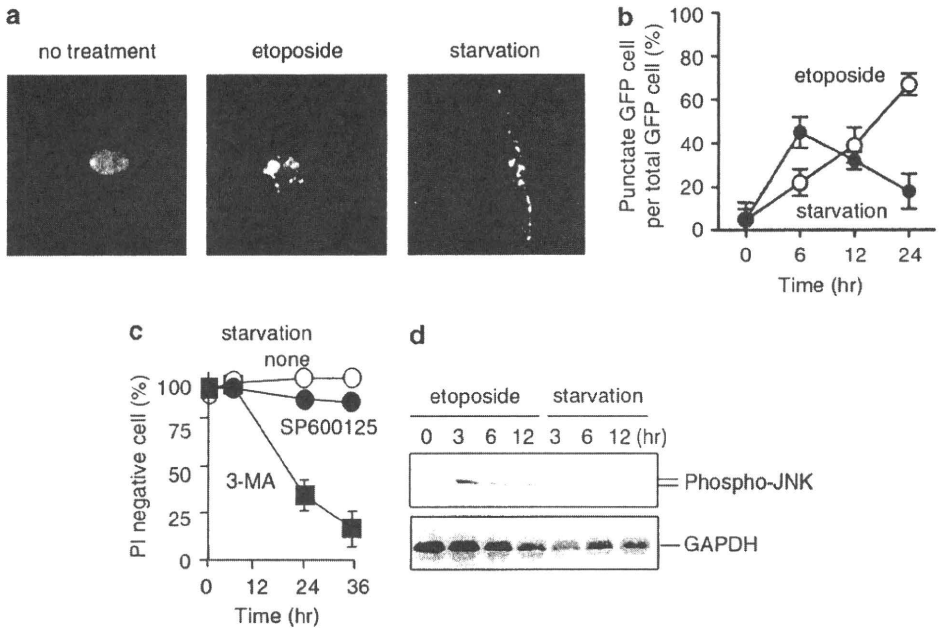

Figure 4 Jun N-terminal kinase (JNK) is not activated by starvation-induced autophagy. (**a**, **b**) Green fluorescent protein–light chain 3 (GFP–LC3)-transfected double-knockout (DKO) mouse embryonic fibroblasts (MEFs) were not treated, treated with 20 μM etoposide, or cultured in nutrient deprivation medium (starvation) for 12 h, and then were examined by fluorescent microscopy. (**a**) Representative photographs of cells showing GFP–LC3 are shown. (**b**) Time-course analysis of autophagic cells during starvation (closed circles) and etoposide treatment (open circles). Data are shown as mean ± s.d. ($n = 4$). (**c**) No autophagic death of starved DKO MEFs. DKO MEFs were cultured in nutrient deprivation medium in the absence (open circles) or presence of 10 mM 3-methyl adenine (3-MA; closed squares) or 25 μM SP600125 (closed circles). Cell viability was then measured by propidium iodide (PI) staining. Data are shown as mean ± s.d. ($n = 4$). (**d**) No activation of JNK by starvation. DKO MEFs were treated with 20 μM etoposide or were cultured in nutrient deprivation medium for the indicated periods. Cell lysates were subjected to immunoblot analysis with an antibody against phosphorylated JNK.

We next questioned whether the combination of autophagy and JNK activation could induce autophagic cell death. To elucidate this, we introduced MKK7–JNK plasmid into DKO MEFs and subjected to starvation. Although starvation or MKK7–JNK transfection alone did not induce cell death in DKO MEFs (Figures 4 and 5b), their combination significantly induced cell death that was greatly inhibited by 3-MA (Figure 5c), suggesting that co-activation of JNK and autophagy induced autophagic cell death.

JNK does not influence etoposide-induced autophagy in Bax/Bak DKO MEFs

As JNK activation was involved in etoposide- and staurosporine-induced autophagic death of Bax/Bak DKO MEFs, we next investigated whether JNK had an influence on autophagic process during the death of these cells. To examine this, GFP–LC3 was first expressed in Bax/Bak DKO MEFs. As a result, etoposide-treated Bax/Bak DKO MEFs showed punctate fluorescence due to the induction of autophagy (Figure 6a). This punctate fluorescence was inhibited by 3-MA, but not SP600125 (Figures 6a and b), although both agents inhibited autophagic cell death. Consistently, the majority of etoposide-treated DKO MEFs contained a number of autophagosomes/autolysosomes, observed with electron microscopy, irrespective of addition of the JNK inhibitor (Figure 6c). Similar results were also obtained using LC-3II formation (Figure 6d), which is a well-established indicator of autophagy (Kabeya *et al.*, 2000). Furthermore, accumulation of Beclin 1, a molecule involved in autophagy, was observed at similar levels in etoposide-treated DKO MEFs in the presence and absence of SP600125 (Figure 6d). Notably, the extent of etoposide-induced autophagy in Bcl-x_L-expressing $sek1^{-/-}$ $mkk7^{-/-}$ cells was the same as that in Bcl-x_L-expressing WT cells, as assessed by LC-3I/II generation (Figure 3d). All of these results indicated that inhibition of JNK suppressed autophagic cell death without affecting the occurrence of autophagy in etoposide-treated Bax/Bak DKO MEFs.

Activation of JNK occurs downstream of autophagy in etoposide-treated Bax/Bak DKO MEFs

Given that activation of JNK was involved in etoposide- and staurosporine-induced autophagic cell death, but not in the process of autophagy itself, we next investigated whether JNK activation occurred downstream of autophagy. We added 3-MA to etoposide-treated Bax/Bak DKO MEFs and then measured the phosphorylation of JNK. Inhibition of autophagy by 3-MA led to a marked reduction in the phosphorylation of JNK in etoposide-treated Bax/Bak DKO MEFs (Figure 7a), suggesting that the occurrence of autophagy was required for the activation of JNK. To confirm this, we used gene silencing with siRNA to inhibit Atg5. As shown in Figure 7b, silencing of Atg5 inhibited the

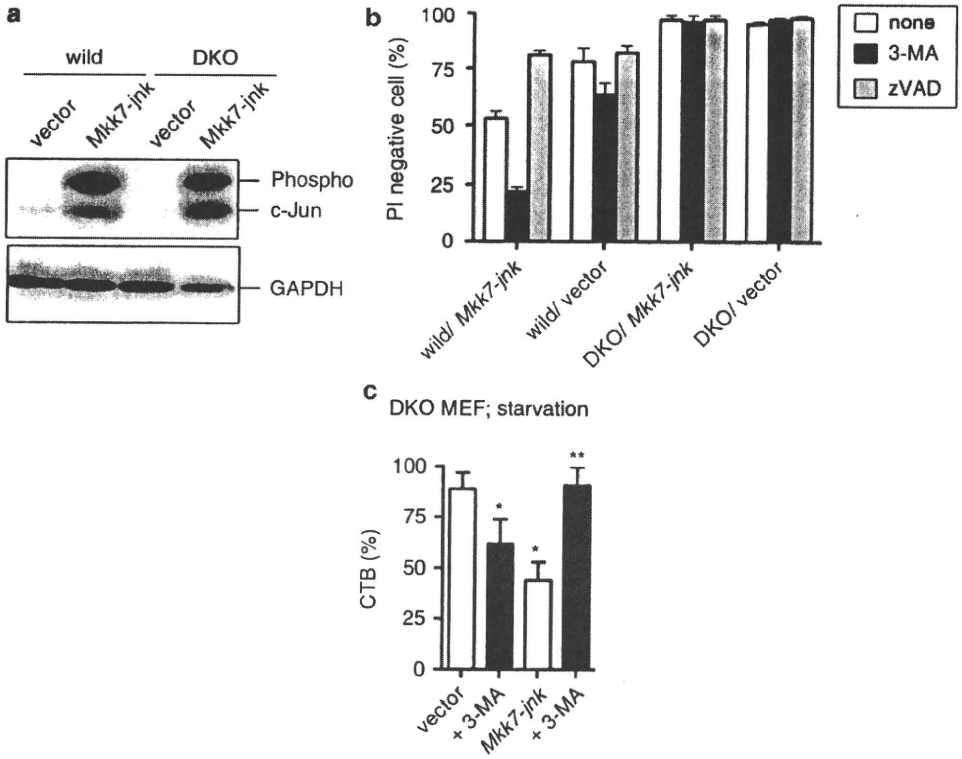

Figure 5 Enforced activation of jun N-terminal kinase (JNK) induced autophagic cell death in starved, but not healthy, Bax/Bak double-knockout (DKO) mouse embryonic fibroblasts (MEFs). **(a)** Wild-type and Bax/Bak DKO MEFs were transiently transfected with DNA encoding the *mkk7-jnk* fusion protein or empty vector for 24 h, and JNK activation was examined. Cell lysates were subjected to immunoblot analysis with an antibody against phosphorylated c-Jun. **(b)** Wild-type and Bax/Bak DKO MEFs were transiently transfected with DNA for the *mkk7-jnk* fusion protein or empty vector in the absence (white columns) or presence of 10 mM 3-methyl adenine (3-MA; black columns) or 100 μM benzyloxycarbonyl-Val-Ala-Asp (OMe) fluoromethylketone (zVAD-fmk; gray columns) for 24 h. Cell viability then was assessed by propidium iodide (PI) staining. Data are shown as mean ± s.d. ($n = 4$). **(c)** Bax/Bak DKO MEFs were transiently transfected with the *mkk7-jnk* fusion plasmid or empty vector. After 24 h, cells were starved in the absence (white columns) or presence of 10 mM 3-MA (black columns) for 24 h. Cell viability then was assessed by Cell Titer Blue (CTB) assay. Data are shown as mean ± s.d. ($n = 4$). Asterisks indicate significant differences at $P < 0.05$ (*vs vector transfection only, **vs *mkk7-jnk* transfection only).

phosphorylation of JNK, similarly to the results obtained using 3-MA. Furthermore, as shown in Figure 7c, activation of JNK was not seen in Bcl-x_L-expressing Atg5$^{-/-}$ MEFs (Kuma *et al.*, 2004), whereas it was observed in Bcl-x_L-expressing Atg5$^{+/+}$ MEFs. The viability of Bcl-x_L-expressing Atg5$^{-/-}$ MEFs was superior to that of Bcl-x_L-expressing Atg5$^{+/+}$ MEFs in response to etoposide, despite the equivalent expression levels of Bcl-x_L (Figure 7d). Therefore, these results indicated that the activation of JNK occurred downstream of the induction of autophagy, and that JNK activation then induced cell death.

Activation of JNK induces autophagic cell death in Bcl-x_L-overexpressing HeLa cells

Finally, we questioned whether JNK-mediated autophagic cell death also occurred in apoptosis-resistant human cancer cells. To examine this, we produced apoptosis-resistant HeLa cells by stably overexpressing Bcl-x_L (designated as HeLa/Bcl-x_L; Figure 8a). In contrast to the etoposide-treated Bax/Bak DKO MEFs, which did not die by apoptosis but lost their viability by autophagic cell death (Figure 2b), HeLa/Bcl-x_L cells maintained their viability in the presence of etoposide (Figure 8b). To elucidate a reason why HeLa/Bcl-x_L cells could avoid the autophagic cell death, we examined the induction of autophagy and JNK activation. Induction of autophagy was observed in etoposide-treated HeLa/Bcl-x_L cells, as assessed by GFP–LC3 (Figure 8d) and LC3-II generation (Figure 8e). In contrast, etoposide-induced JNK activation in Hela/Bcl-x_L cells was much weaker than that in etoposide-treated DKO MEFs (Figure 8f). Therefore, we hypothesized that the lower levels of JNK activation in Hela/Bcl-x_L cells was responsible for their resistance to autophagic cell death. To examine this possibility, we introduced *mkk7-jnk* expression plasmid into HeLa/Bcl-x_L cells (Figure 8c) and treated the cells with etoposide. In response to etoposide, *mkk7-jnk*-transfected HeLa/Bcl-x_L cells showed autophagy induction (Figures 8d and e) and lost their viability, which was inhibited by 3-MA (Figure 8g), suggesting the occurrence of autophagic cell death. Taken together, co-activation of autophagy and JNK is crucial for the induction of autophagic cell death.

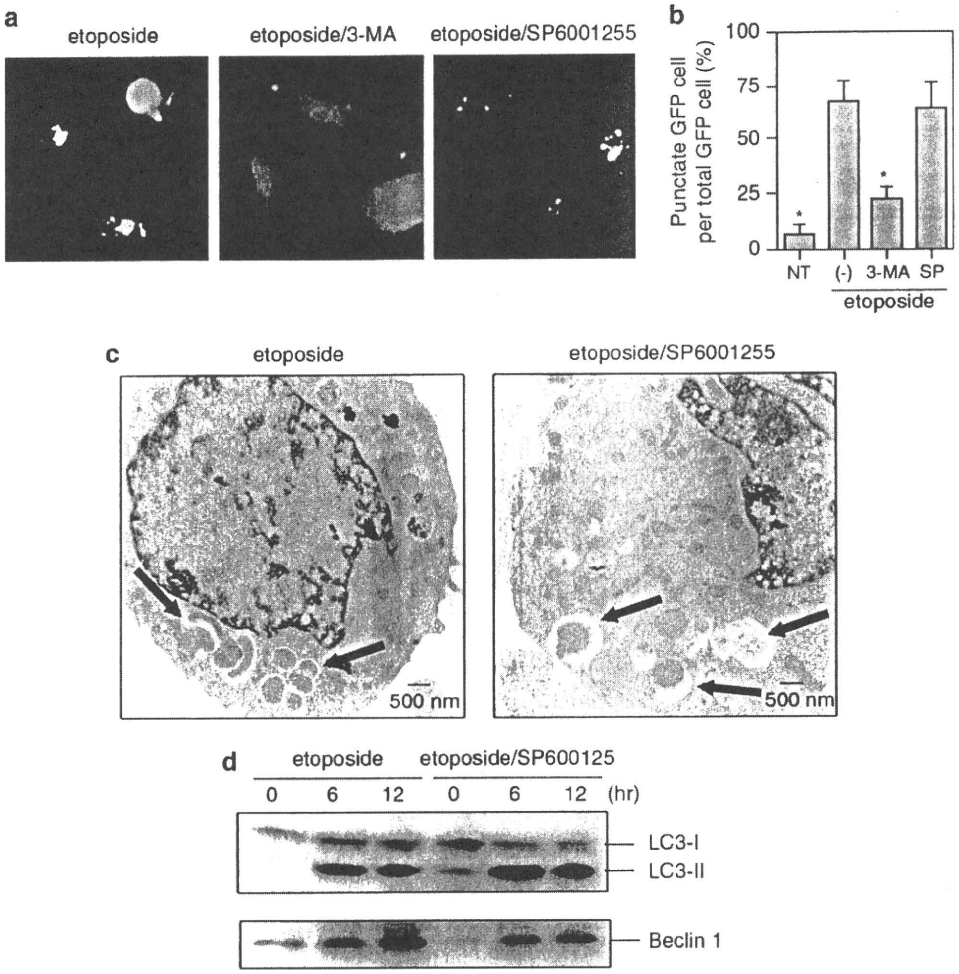

Figure 6 No effect of a jun N-terminal kinase (JNK) inhibitor on etoposide-induced autophagy of Bax/Bak double-knockout (DKO) mouse embryonic fibroblasts (MEFs). (**a**, **b**) Green fluorescent protein–light chain 3 (GFP–LC3)-transfected DKO MEFs were treated with 20 μM etoposide in the absence or presence of 25 μM SP600125 (SP) or 10 mM 3-methyl adenine (3-MA) for 24 h, and then were examined by fluorescent microscopy. Representative photographs are shown in (**a**), and the percentage of cells with punctate GFP relative to all GFP-positive cells is indicated in (**b**). Data are shown as mean ± s.d. ($n = 4$). Asterisks indicate a significant difference at $P < 0.05$ (vs etoposide only). (**c**) Representative electron micrograph of Bax/Bak DKO MEFs treated with etoposide for 18 h in the presence or absence of SP600125. Arrows indicate autophagosomes/autolysosmes. (**d**) DKO MEFs were treated with 20 μM etoposide in the absence or presence of 25 μM SP600125 for the indicated periods. Then cell lysates were subjected to immunoblot analysis with an antibody against LC3 and Beclin 1.

Discussion

Autophagic cell death is thought to be involved in various physiological and pathological events. However, it has long been assessed only from the point of view of morphological changes due to lack of knowledge regarding the molecular events involved in this process, making it difficult to fully understand the role of autophagic cell death *in vivo*. Recently, Lenardo and colleagues and our group reported different experimental systems, in which autophagic cell death could be activated, which were suitable for investigating the molecular mechanisms of autophagic cell death (Shimizu *et al*., 2004; Yu *et al*., 2004). Although the two cellular systems are different, they may share the core machinery of autophagic cell death. Lenardo and colleagues reported that caspase-8, JNK and degradation of catalase were involved in the autophagic death of zVAD-fmk-treated L929 cells (Yu *et al*., 2004, 2006). Our preliminary studies excluded the involvement of caspase-8 and catalase in the autophagic death of Bax/Bak DKO cells, as the extent of autophagic cell death was equal in Bcl-x_L-overexpressing caspase-8-deficient MEFs and Bcl-x_L-overexpressing wild-type MEFs after etoposide stimulation (Shimizu, unpublished data), and as significant degradation of catalase was not observed in etoposide-treated Bax/Bak DKO MEFs (Shimizu, unpublished data). In contrast, involvement of JNK seems to be common to both of these autophagic cell death systems. This study showed that: (1) JNK is activated when autophagic cell death is induced in Bax/Bak DKO MEFs by etoposide and staurosporine, but not when cells are starved; (2) autophagic cell death is suppressed by inhibition of JNK; (3) activation of JNK is required (but not sufficient) for autophagic cell death; and (4) activation of JNK is largely dependent on the

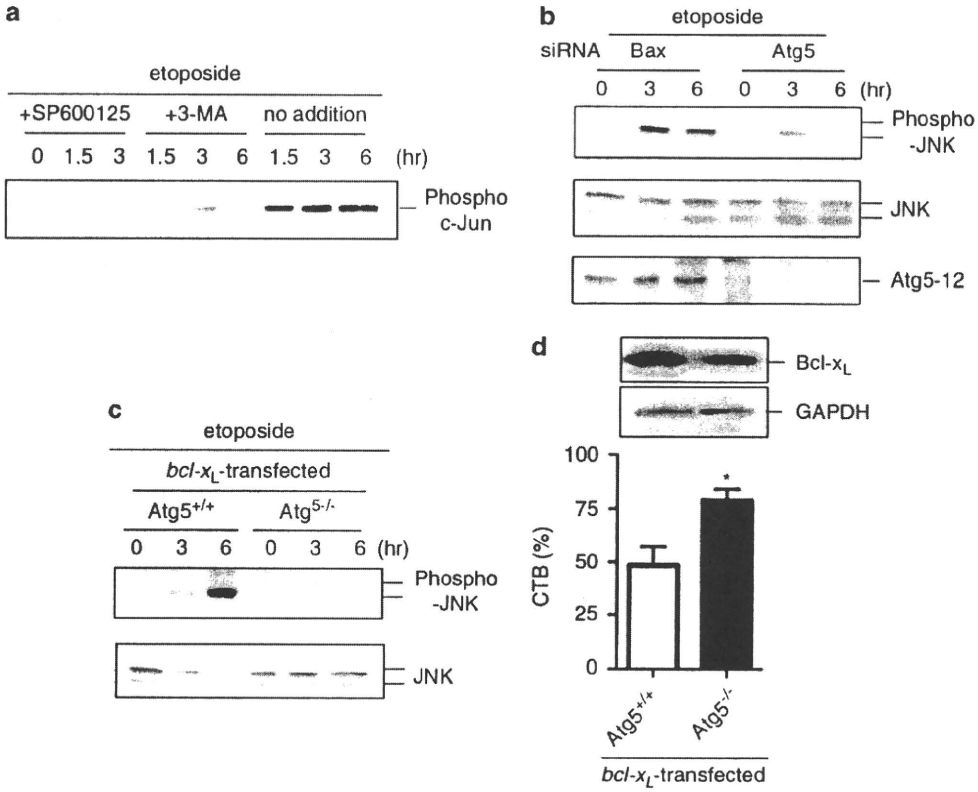

Figure 7 Involvement of autophagy in etoposide-induced activation of JNK in double-knockout (DKO) mouse embryonic fibroblasts (MEFs). (**a**) DKO MEFs were treated with 20 μM etoposide in the absence or presence of 25 μM SP600125 or 10 mM 3-methyl adenine (3-MA) for the indicated periods. Cell lysates were subjected to an *in vitro* c-Jun kinase assay by western blotting using an anti-phosphorylated c-Jun antibody. (**b**) DKO MEFs were treated with the indicated small interfering RNAs (siRNAs) for 24 h and then incubated with 20 μM etoposide for the indicated periods. Cell lysates were subjected to western blotting with anti-phosphorylated JNK, anti-JNK and anti-Atg5 (Atg5-12) antibodies. (**c**, **d**) $Atg5^{+/+}$ and $Atg5^{-/-}$ MEFs were transfected with the *bcl-x*$_L$ complementary DNA for 24 h and then incubated with 20 μM etoposide for the indicated periods. Cell lysates were subjected to western blotting with anti-phosphorylated JNK antibodies, anti-JNK antibodies (**c**) and Bcl-x_L (**d**). Glyceraldehyde 3-phosphate dehydrogenase (GAPDH) is used as a loading control. Cell viability was assessed by the Cell Titer Blue (CTB) assay (**d**). Data are shown as mean ± s.d. ($n = 4$). Asterisks indicate a significant difference at $P < 0.05$.

autophagic process. These results indicate that JNK is involved in autophagic cell death without influencing the process of autophagy itself, which could be an important piece of information regarding the molecular mechanisms of autophagic cell death.

Jun N-terminal kinase belongs to the mitogen-activated protein kinases and is activated by apoptosis signal-regulating kinase 1 (mitogen-activated protein kinase kinase kinase) and SEK1/MKK7 (mitogen-activated protein kinase kinase) when cells are exposed to various stresses (Davis, 2000). The role of JNK in cell death has long been studied. The activation of JNK is observed when apoptosis is induced by various stressors, including ultraviolet irradiation and tumor necrosis factor, but its function has long been controversial, as it has a pro-apoptotic role in some physiological and pathological conditions, whereas it exerts an anti-apoptotic effect in other situations (Davis, 2000). However, at least, part of this complex issue has been explained by the discovery of different modes of JNK activation (Ventura *et al.*, 2006). The early transient phase of JNK activation signals for cell survival, whereas sustained JNK activation can trigger apoptotic signals. Sustained activation of JNK has also been reported to mediate reactive oxygen species-induced necrosis (Nakano *et al.*, 2006). Similarly, we observed the sustained activation of JNK for more than 6 h (Figure 1) in Bax/Bak DKO MEFs undergoing etoposide-induced autophagic cell death. Therefore, sustained JNK activation seems to be harmful for cells.

How does sustained JNK activation induce cell death? In the case of necrosis, JNK has been reported to act as a positive regulator of reactive oxygen species production (Nakano *et al.*, 2006), although the precise mechanisms involved are unclear. The mechanisms that account for pro-apoptotic signaling by JNK have been studied extensively, and various downstream molecules have been proposed. In neurons, especially in developing neurons, JNK induces apoptosis by activating c-jun-mediated transcription (Behrens *et al.*, 1999). In other cells, however, JNK-mediated apoptosis does not require *de novo* protein synthesis because direct phosphorylation of target molecules induces apoptosis (Tournier *et al.*, 2000). In any case, JNK functions upstream of apoptotic mitochondrial changes, so that the absence of Bax and Bak blocks JNK-mediated apoptosis. This was confirmed

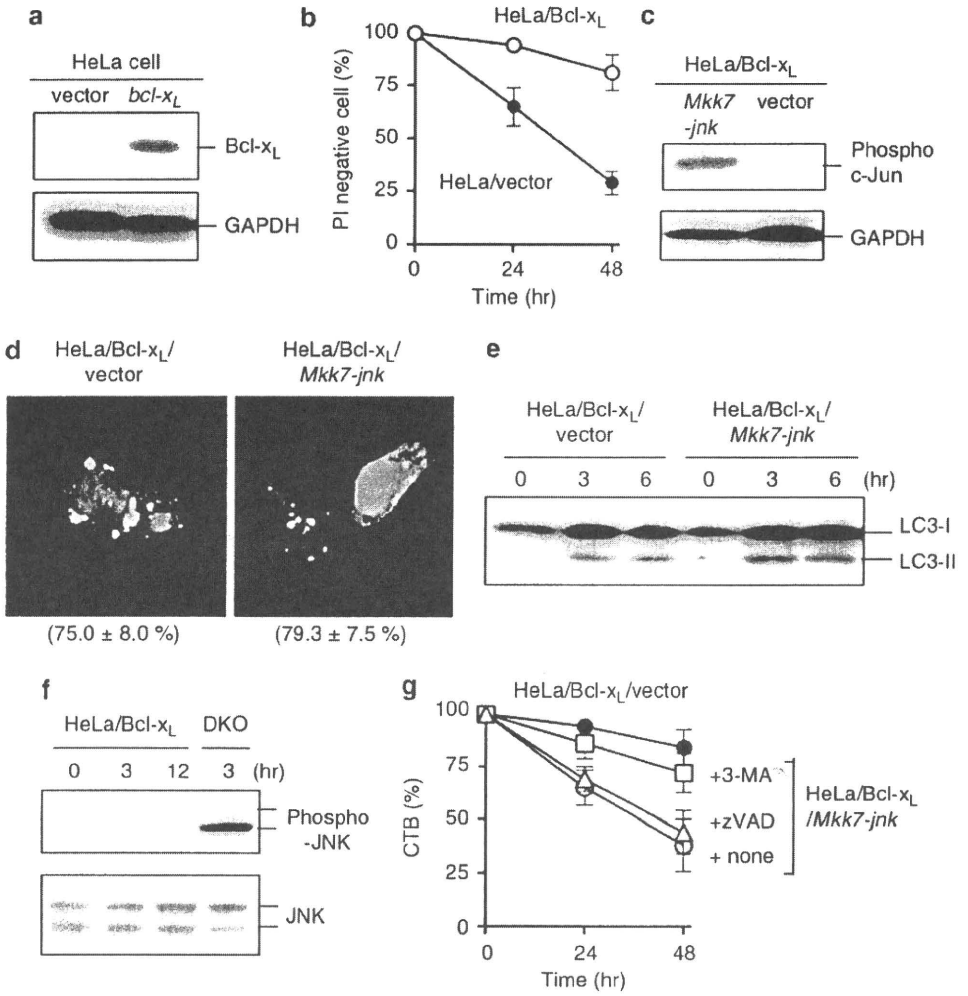

Figure 8 Induction of autophagic cell death in HeLa/Bcl-xL cells by co-activation of jun N-terminal kinase (JNK) and autophagy. (**a**, **b**) HeLa cells were stably transfected with the human *bcl-x*$_L$ plasmid or empty vector. Cell lysates were subjected to immunoblot analysis with an antibody against human Bcl-x$_L$ (**a**). Cells were treated with 100 μM etoposide for the indicated hours and viability was assessed by propidium iodide (PI) staining (**b**). Data are shown as mean ± s.d. ($n = 4$). (**c**) HeLa/Bcl-x$_L$ cells were transiently transfected with DNA for the *mkk7-jnk* fusion protein or empty vector for 24 h, and JNK activation was examined. Cell lysates were subjected to immunoblot analysis with an antibody against phosphorylated c-Jun. (**d**, **e**) HeLa/Bcl-x$_L$ cells were transiently transfected with DNA for the *mkk7-jnk* fusion protein or empty vector together with green fluorescent protein light chain 3 (GFP–LC3) plasmid for 24 h, then cells were treated with 100 μM etoposide for 6 h. (**d**) Representative photographs and the percentage of cells with punctate GFP relative to all GFP-positive cells are shown. Data are shown as mean ± s.d. ($n = 4$). (**e**) Cell lysates were subjected to immunoblot analysis with an antibody against LC3. (**f**) Weak activation of JNK in etoposide-treated HeLa/Bcl-x$_L$ cells. HeLa/Bcl-x$_L$ cells were treated with 100 μM etoposide for the indicated periods. Cell lysates were subjected to immunoblot analysis with an antibody against phosphorylated JNK and JNK. As a positive control, lysates from Bax/Bak double-knockout (DKO) mouse embryonic fibroblasts (MEFs) treated with 20 μM etoposide for 3 h were used. These antibodies equivalently cross-react with human and mouse proteins. (**g**) HeLa/Bcl-x$_L$ cells were transiently transfected with DNA for the *mkk7-jnk* fusion protein (open symbols) or empty vector (closed symbols) for 24 h, then cells were treated with 100 μM etoposide in the absence (circles) or presence of 10 mM 3-MA (squares) or 100 μM benzyloxycarbonyl-Val-Ala-Asp (OMe) fluoromethylketone (zVAD-fmk; triangles) for 48 h. Cell viability was assessed by Cell Titer Blue (CTB) assay. Data are shown as mean ± s.d. ($n = 4$).

by our findings that over-activation of JNK induced the apoptosis of wild-type MEFs, but not of Bax/Bak DKO MEFs (Figure 5). These data also suggested the possibility that Bcl-2 family members could be direct target(s) of JNK. Actually, JNK induces the expression of BH3-only proteins: Hrk and Bim (Harris and Johnson, 2001). Jun N-terminal kinase also phosphorylates Bcl-2 family members and promotes pro-apoptotic Bax activity (Kim *et al.*, 2006), and inhibits various anti-apoptotic Bcl-2 family members, including Bcl-2, Bcl-x$_L$ and Mcl-1 (Ito *et al.*, 1997; Park *et al.*, 1997). In addition, JNK indirectly determines the activation of Bax through its regulation of 14-3-3 (Tsuruta *et al.*, 2004). Thus, the Bcl-2 family proteins are considered to be likely targets of JNK during the process of apoptosis. With regard to autophagic cell death, we have previously reported that Bcl-x$_L$ may regulate the autophagic death of etoposide-treated DKO MEFs (Shimizu *et al.*, 2004), so this molecule might be a target when JNK activates autophagic cell death.

The molecular mechanism of JNK activation is another crucial issue with regard to understanding

autophagic cell death. We found several pieces of evidence that suggest that the activation of JNK largely occurs in an autophagy-dependent manner: (1) 3-MA-mediated inhibition of autophagy suppressed JNK activation (Figure 7a), (2) silencing of the *Atg5* gene also suppressed JNK activation (Figure 7b), and (3) JNK activation was weaker in Bcl-x_L-overexpressing $Atg5^{-/-}$ MEFs than in Bcl-x_L-overexpressing $Atg5^{+/+}$ MEFs (Figure 7c). These results indicate that activation of the autophagic process can activate JNK, but induction of autophagy does not necessarily lead to JNK activation. Whether autophagy activates JNK seems to depend on the stimulus, as etoposide and staurosporine, but not starvation, induced JNK activation as shown in this study. Why does JNK activation occur during etoposide/staurosporine-induced autophagic cell death, but not during starvation, although autophagy is activated in both cases? There are two possibilities that can be suggested. We have previously shown that some autophagic proteins, including Atg5 and Beclin 1, are upregulated during etoposide/staurosporine-induced autophagic cell death, but not during starvation (Shimizu *et al*., 2004). Therefore, a difference in the level of autophagic activity may determine whether JNK activation occurs. Alternatively, other signals in addition to autophagy itself might be required for the activation of JNK. In any case, autophagy may activate endoplasmic reticulum stress or oxidative stress during digestion of endoplasmic reticulum or mitochondria, which may activate JNK signaling pathway.

In contrast to our findings, several investigators have described that JNK activation occurred upstream of the induction of autophagy or autophagic cell death when various cells are starved (Wei *et al*., 2008), treated with tumor necrosis factor (Cheng *et al*., 2008) and ceramide (Li *et al*., 2009). Possible explanation for this discrepancy might be the difference of the cell types or stimuli used. Tumor necrosis factor and oxidative stress directly activate JNK through tumor necrosis factor receptor-associated factor 2 and apoptosis signal-regulating kinase 1, respectively. In contrast, other signals, such as etoposide, could not directly activate JNK. In such case, JNK activation may be dependent on the environmental and genetic circumstances. Further studies will be necessary to address this issue.

Materials and methods

Antibodies and chemicals

Anti-phospho c-Jun (Ser63)II, anti-stress-activated protein kinase/JNK, anti-phospho p38, anti-phospho stress-activated protein kinase/JNK (Thr183/Tyr185), anti-phospho ERK1/2 and anti-phospho ERK5 antibodies were obtained from Cell Signaling Technologies (Danvers, MA, USA). Anti-Bcl-x_L (S-18), anti-active caspase-3 and anti-LC3 polyclonal antibodies were purchased from Santa Cruz Biotechnology (Santa Cruz, CA, USA), Promega (Madison, WI, USA) and MBL (Nagoya, Japan), respectively. A stress-activated protein kinase/JNK Kinase Assay Kit (nonradioactive) was purchased from Cell Signaling Technologies. The inhibitors SP600125 and SB203580 were obtained from Tocris Bioscience (Ellisville, MO, USA). Cell Titer Blue and 3-MA were purchased from ICN Biochemicals (Irvine, CA, USA) and Promega, respectively. Other chemicals were purchased from Wako (Osaka, Japan).

Cell culture and DNA transfection

$Bax^{-/-}Bak^{-/-}$ (DKO), $Atg5^{-/-}$ and $Atg5^{+/+}$ MEFs were collected from mouse embryos at E14.5, and immortalized with Simian virus 40 T antigen (Shimizu *et al*., 2004). Mouse embryonic fibroblasts were cultured in Dulbecco's modified Eagle's medium supplemented with 2 mM L-glutamine, 1 mM sodium pyruvate, 0.1 mM non-essential amino acids, 10 mM HEPES/Na^+, (pH 7.4), 0.05 mM 2-mercaptoethanol, 100 U/ml penicillin, 100 μg/ml streptomycin and 10% fetal bovine serum. Sek1/MKK7 double-knockout embryonic stem cells were used as MEF-like cells, and were cultured as described previously (Nishitai *et al*., 2004). For starvation of cells, culturing was done in Hanks' balanced salt solution supplemented with 1 mM sodium pyruvate, 10 mM HEPES/Na^+ (pH 7.4) and 0.05 mM 2-mercaptoethanol. HeLa/Bcl-x_L cells were generated by transfection of the expression plasmid for human Bcl-x_L.

The plasmids pCMV5-JNK1 APF (the mammalian expression plasmid for dominant-negative JNK; Gupta *et al*., 1995), pCDNA3 MKK7-JNK1 WT (the mammalian expression plasmid for the MKK7–JNK1 fusion gene; Gupta *et al*., 1995) and pCAGGS-GFP-LC3 (Kabeya *et al*., 2000) were kindly provided by Drs R Davis, Y Gotoh and N Mizushima, respectively. The pUC-CAGGS expression vector with DNA encoding human Bcl-x_L has been described earlier (Shimizu *et al*., 1996). Cells (1×10^6) were transfected with plasmid DNA using the Amaxa electroporation system according to the supplier's protocol (kit V, program U-20). The transfection efficiency was more than 75%, as assessed by co-transfection with DNA expressing GFP. All siRNAs were produced by Dharmacon Research. The sequences used are as follows (numbers in parentheses indicate nucleotide positions within the respective open reading frames): mouse Atg5 siRNA: 5′-AACUUGCUUUACUCUCUAUCA-3′ (51–71). Cells (1×10^6) were transfected with 10 μg of siRNA using the Amaxa electroporation system.

Analysis of mitogen-activated protein kinase activation

Cells were seeded into 6-well dishes at a density of 3.5×10^6 cells per well. After 24 h, cells were treated with etoposide (20 μM), staurosporine (1 μM), ultraviolet irradiation (100 J/m^2), or were nutrient deprived in the presence or absence of SP600125 (25 μM) and 3-MA (10 mM). The *in vitro* kinase assay was performed according to the supplier's protocol. Briefly, cell lysates were mixed with c-Jun fusion protein-coated agarose beads at 4 °C for 12 h. After centrifugation and washing, beads were suspended in the Kinase Buffer supplemented with 200 mM ATP for 30 min at 30 °C. Then phosphorylated c-Jun was detected with an anti-phospho-c-Jun antibody. The activation of JNK was also evaluated by western blotting using an anti-phospho JNK monoclonal antibody. The activation of p38, ERK1/2 and ERK5 was assessed by western blotting.

Cell viability assay

Cells were seeded into 6-well dishes at a density of 3.5×10^6 cells per well. After 24 h, cells were exposed to etoposide (20 μM), staurosporine (1 μM) or were nutrient deprived in the presence or absence of SP600125, SB203580, 3-MA or z-VAD-fmk at the indicated concentrations. Cells, including floating cells, were then collected and viability was assessed by propidium iodide (PI) staining or CTB assay (Shimizu *et al*.,

2004). Briefly, cells were stained with 1 μM PI for 5 min at room temperature, and then were analyzed using a flow cytometer (FACS Caliber; Becton-Dickinson, Franklin Lakes, NJ, USA). The CTB assay was carried out using Cell Titer Blue assay reagent according to the supplier's protocol.

To examine proliferative activity, MEFs were treated with etoposide, all the cells were recovered, and then, 5000 or 10 000 cells were re-cultured in standard medium in 96-well or 48-well dishes, respectively. Viable cells were measured on the indicated days by the CTB assay (Shimizu *et al.*, 2004). For the colony formation assay, MEFs were treated with etoposide, collected and 2000 cells were seeded into 24-well dishes containing standard medium. After 1 week, the number of colonies was counted (Shimizu *et al.*, 2004).

Western blot analysis
Whole-cell protein extracts were prepared using RIPA buffer, and the protein content was quantified by Lowry's method (Bio-Rad, Tokyo, Japan) according to the manufacturer's instructions. Proteins were then separated by electrophoresis on 15% sodium dodecyl sulfate–polyacrylamide gels and transferred to polyvinylidene fluoride membranes. Filters were treated with the indicated antibodies and proteins were detected using the appropriate horseradish peroxidase-conjugated secondary antibodies and enhanced chemiluminescent reagent (GE healthcare Japan, Tokyo, Japan).

Staining of autophagosomes and lysosomes/autolysosomes
Cells were transfected with 1 μg of GFP–LC3 expression plasmid (Kabeya *et al.*, 2000). After 24 h, cells were subjected to etoposide treatment or starvation and GFP–LC3 fluorescence was observed under a confocal fluorescence microscope (LSM 510 META, Zeiss Japan, Tokyo, Japan).

Electron microscopy
Cells were fixed with 2% paraformaldehyde/2% glutaraldehyde in 0.1 M phosphate buffer (pH 7.4), followed by fixing in 1% OsO_4. After dehydration, ultrathin sections were stained with uranyl acetate and lead citrate for observation under a JEM 100 CX electron microscope (JEOL, Tokyo, Japan).

Conflict of interest

The authors declare no conflict of interest.

Acknowledgements

We thank Dr N Mizushima for providing us with MEFs from Atg5$^{-/-}$ and Atg5$^{+/+}$ mice and pCAGGS-GFP-LC3 plasmid. We also thank Drs R Davis and Y Gotoh for providing PCMV5-JNK1 APF plasmid and pCDNA3 MKK7-JNK1 WT plasmid, respectively. This study was partly supported by the Program for Promotion of Fundamental Studies in Health Sciences of the National Institute of Biomedical Innovation (NIBIO); a grant for Scientific Research on Priority Areas, SORST of Japan Science and Technology Corp; a grant for the 21st Century COE Program; a grant for Creative Scientific Research from the Japanese Ministry of Education, Science, Sports and Culture; and a grant for Comprehensive Research on Aging and Health from the Japanese Ministry of Health, Labor and Welfare. This study was also supported by grants from the Uehara Memorial Foundation and the Naito Foundation.

References

Baehrecke EH. (2002). How death shapes life during development. *Nat Rev Mol Cell Biol* **3**: 779–787.

Behrens A, Sibilia M, Wagner FF. (1999). Amino-terminal phosphorylation of c-Jun regulates stress-induced apoptosis and cellular proliferation. *Nat Genet* **21**: 326–329.

Boya P, Gonzalez-Polo RA, Casares N, Perfettini JL, Dessen P, Larochette N *et al.* (2005). Inhibition of macroautophagy triggers apoptosis. *Mol Cell Biol* **25**: 1025–1040.

Cheng Y, Qiu F, Tashiro S, Onodera S, Ikejima T. (2008). ERK and JNK mediate TNFalpha-induced p53 activation in apoptotic and autophagic L929 cell death. *Biochem Biophys Res Commun* **376**: 483–488.

Clarke PG. (1990). Developmental cell death: morphological diversity and multiple mechanisms. *Anat Embryol (Berl)* **181**: 195–213.

Davis RJ. (2000). Signal transduction by the JNK group of MAP kinases. *Cell* **103**: 239–252.

Gupta S, Campbell D, Derijard B, Davis RJ. (1995). Transcription factor ATF2 regulation by the JNK signal transduction pathway. *Science* **267**: 389–393.

Harris CA, Johnson Jr EM. (2001). BH3-only Bcl-2 family members are coordinately regulated by the JNK pathway and require Bax to induce apoptosis in neurons. *J Biol Chem* **276**: 37754–37760.

Ito T, Deng X, Carr B, May WS. (1997). Bcl-2 phosphorylation required for anti-apoptosis function. *J Biol Chem* **272**: 11671–11673.

Kabeya Y, Mizushima N, Ueno T, Yamamoto A, Kirisako T, Noda T *et al.* (2000). LC3, a mammalian homologue of yeast Apg8p, is localized in autophagosome membranes after processing. *EMBO J* **19**: 5720–5728.

Kim BJ, Ryu SW, Song BJ. (2006). JNK- and p38 kinase-mediated phosphorylation of Bax leads to its activation and mitochondrial translocation and to apoptosis of human hepatoma HepG2 cells. *J Biol Chem* **281**: 21256–21265.

Klionsky DJ. (2005). Autophagy. *Curr Biol* **15**: R282–R283.

Kuma A, Hatano M, Matsui M, Yamamoto A, Nakaya H, Yoshimori T *et al.* (2004). The role of autophagy during the early neonatal starvation period. *Nature* **432**: 1032–1036.

Levine B, Yuan J. (2005). Autophagy in cell death: an innocent convict? *J Clin Invest* **115**: 2679–2688.

Li DD, Wang LL, Deng R, Tang J, Shen Y, Guo JF *et al.* (2009). The pivotal role of c-Jun NH2-terminal kinase-mediated Beclin 1 expression during anticancer agents-induced autophagy in cancer cells. *Oncogene* **28**: 886–898.

Mizushima N, Ohsumi Y, Yoshimiri T. (2002). Autophagosome formation in mammalian cells. *Cell Struct Funct* **6**: 421–429.

Nakano H, Nakajima A, Sakon-Komazawa S, Piao JH, Xue X, Okumura K. (2006). Reactive oxygen species mediate crosstalk between NF-kappaB and JNK. *Cell Death Differ* **5**: 730–737.

Nishitai G, Shimizu N, Negishi T, Kishimoto H, Nakagawa K, Kitagawa D *et al.* (2004). Stress induces mitochondria-mediated apoptosis independent of SAPK/JNK activation in embryonic stem cells. *J Biol Chem* **279**: 1621–1626.

Ohsumi Y. (2001). Molecular dissection of autophagy: two ubiquitin-like systems. *Nat Rev Mol Cell Biol* **2**: 211–216.

Park J, Kim I, Oh YJ, Lee K, Han PL, Choi EJ. (1997). Activation of c-Jun N-terminal kinase antagonizes an anti-apoptotic action of Bcl-2. *J Biol Chem* **272**: 16725–16728.

Shimizu S, Eguchi Y, Kamiike W, Matsuda H, Tsujimoto Y. (1996). Bcl-2 expression prevents activation of the ICE protease cascade. *Oncogene* **12**: 2251–2257.

Shimizu S, Kaneseki T, Mizushima N, Mizuta K, Arakawa-Kobayashi S, Thompson CB *et al.* (2004). Role of Bcl-2 family proteins in a non-apoptotic programmed cell death dependent on autophagy genes. *Nat Cell Biol* **6**: 1221–1228.

Tournier C, Hess P, Yang DD, Xu J, Turner TK, Nimnual A *et al.* (2000). Requirement of JNK for stress-induced activation of the cytochrome *c*-mediated death pathway. *Science* **88**: 870–874.

Tsuruta F, Sunayama J, Mori Y, Hattori S, Shimizu S, Tsujimoto Y *et al.* (2004). JNK promotes Bax translocation to mitochondria through phosphorylation of 14-3-3 proteins. *EMBO J* **23**: 1889–1899.

Ventura JJ, Hubner A, Zhang C, Flavell RA, Shokat KM, Davis RJ. (2006). Chemical genetic analysis of the time course of signal transduction by JNK. *Mol Cell* **21**: 701–710.

Yu L, Alva A, Su H, Dutt P, Freundt E, Welsh S *et al.* (2004). Regulation of an ATG7-beclin 1 program of autophagic cell death by caspase-8. *Science* **304**: 1500–1502.

Yu L, Wan F, Dutta S, Welsh S, Liu Z, Freundt E *et al.* (2006). Autophagic programmed cell death by selective catalase degradation. *Proc Natl Acad Sci USA* **103**: 4952–4957.

Wei Y, Pattingre S, Sinha S, Bassik M, Levine B. (2008). JNK1-mediated phosphorylation of Bcl-2 regulates starvation-induced autophagy. *Mol Cell* **30**: 678–688.